Heat and Mass Transfer in Co-Current Gas-Liquid Packed Beds Analysis, Recommendations and New Correlations

ARTICLE *in* INDUSTRIAL & ENGINEERING CHEMISTRY RESEARCH · NOVEMBER 2002

Impact Factor: 2.59 · DOI: 10.1021/ie020416g

CORRELATIONS

Heat and Mass Transfer in Cocurrent Gas−Liquid Packed Beds. Analysis, Recommendations, and New Correlations

Faïçal Larachi,* Lamia Belfares, Ion Iliuta, and Bernard P. A. Grandjean

Department of Chemical Engineering & CERPIC, Laval University, Québec, Canada G1K 7P4

Meticulous inspection of the literature has unveiled the weakness of several empirical methods for predicting the macroscopic mass- and heat-transfer characteristics relevant to gas−liquid cocurrent downflow and upflow packed-bed reactors. In response, using a wide experimental database consisting of 5279 measurements for trickle beds (downflow) and 1974 measurements for packed bubble columns (upflow), a set of reliable correlations has been recommended for the prediction of the gas−liquid interfacial area (a_{gl}), the volumetric liquid- (k_la) and gas-side (k_ga) mass-transfer coefficients, the wall ($\eta_e k_{lw}$) and bed ($\eta_e k_{ls}$) liquid−solid mass-transfer coefficients, the wall heat-transfer coefficient (h_w), the bed effective radial thermal conductivity (λ_e), and the particle-to-fluid heat-transfer coefficient (h_p). Some of these correlations are from the literature, and others have been developed by combining artificial neural networks and dimensional analysis. The accuracy of the proposed correlations surpasses by far the performances of the available methods sometimes by up to a 10-fold reduction in scatter. Notwithstanding the substantial reduction in scatter, these correlations have been thoroughly tested for phenomenological consistency and have been shown to restore the expected trends documented in the database.

Introduction

Over the past 40 years, gas−liquid cocurrent contacting in catalytic packed-bed reactors, trickle beds, and packed bubble columns alike has achieved widespread acceptance in a great deal of industrial applications.[1,2] Though two such configurations, i.e., downflow for the former and upflow for the latter, are traditionally ubiquitous in the petroleum and petrochemical industries, they are effective for hosting other catalyst-mediated reactions such as those for the production of commodity and specialty chemicals, pharmaceuticals, pesticides, and herbicides, for waste treatment and bioscrubbing, and in biochemical and electrochemical processing.[3−10]

This contribution continues a series of papers devoted to the database building, correlations' development, and analyses of the macroscopic transport of momentum, heat, and mass in two-phase-flow packed beds. The endeavor is envisioned from the perspective of the inherited body of knowledge acquired over the past half a century in the realm of multiphase reactors. The long-term objective is to formulate more efficient design tools for the reliable estimation of the transport parameters validated over the broadest data repositories or, by default, to orient experiments in new uncovered domains where existing correlations fail to forecast or are simply nonexistent.

Despite considerable research, the knowledge about the mass and heat transfer in trickle beds and packed bubble columns is still not well standardized, and general correlations of mass- and heat-transfer parameters are still to be established. The mass-transfer parameters we are interested in here are the volumetric liquid- and gas-film mass-transfer coefficients, k_la and k_ga, the gas−liquid interfacial area, a_{gl}, the liquid−(particle)solid mass-transfer coefficients, $\eta_e k_{ls}$, and the liquid−(column)wall mass-transfer coefficients, $\eta_e k_{lw}$. Furthermore, the heat-transfer coefficients that are considered are the bed effective radial thermal conductivity, λ_e, the wall heat-transfer coefficient, h_w, and the particle-to-fluid heat-transfer coefficient, h_p.

The present work aims at providing researchers and engineers with very accurate correlations for the above-cited mass- and heat-transfer parameters in cocurrent packed-bed reactors. After a brief display of the heat- and mass-transfer databases in the first section, the methodology used to develop the new correlations is quickly highlighted in the second section, which is followed by section three, where the most important correlations to predict mass- and heat-transfer parameters are confronted to the databases and statistically ranked at the merit. Such correlations either can come from the open literature or are developed herein using neural network computing. The last section deals with a discussion of the parametric trends of the best correlations in view of the behavior of the macroscopic transport parameters as reported in the laboratory from their experimental measurements.

Database Display

In view of its broad coverage of the literature, the present study brings together a vast majority of data

* Corresponding author. E-mail: flarachi@gch.ulaval.ca. Tel: 1-418-656-3566. Fax: 1-418-656-5993.

10.1021/ie020416g CCC: $25.00
Published on Web 11/20/2002

Table 1. Intervals of Operating Conditions for the Mass-Transfer Database in the Downflow Mode

category	properties	a_{gl} range	$k_l a$ range	$k_g a$ range	$\eta_e k_{ls}$ range	$\eta_e k_{lw}$ range
operating conditions	pressure (P; MPa)	0.1−5	0.1−3.1	0.1	0.1−3.5	0.1−9
	temperature (T; K)	293−313	286−313	290−299	286−323	298−303
	superficial velocity ($v_{sl} \times 10^2$; m/s)	5.8×10^{-2}−12.6	6.66×10^{-5}−15	4.56×10^{-2}−1.62	2.6×10^{-2}−24.45	0.2−5
	superficial velocity ($v_{sg} \times 10^2$; m/s)	0.84−450	0.15−450	0.38−200	0−246	0.1−47
	v_{sg}/v_{sl}	0.23−1454	0.064−6219	0.74−1819	0−3808	0−126.9
packing and bed properties	particle diameter ($d_p \times 10^3$; m)	1.16−34.7	0.541−20	0.541−22	0.45−12.7	5
	bed porosity (ϵ)	0.243−0.94	0.356−0.89	0.273−0.93	0.31−0.63	0.4
	bed specific surface area (a_t; m^{-1})	147−3805.5	243−6070	190.3−6070	275−8535	720−762
	sphericity factor (ϕ)	0.126−1	0.133−1	0.139−1	0.407−1	1
	material wettability[a]	+ and −	+ and −	+	+	+
	packed bed height (H; m)	0.1−3.26	0.042−1.4	0.127−0.92	0.02−2.4	0.8−1.3
	column diameter ($d_c \times 10^2$; m)	2.3−38	1.58−17.2	2.58−15.24	1.5−17.2	5−7
liquid properties	density (ρ_l;[b] kg/m^3)	805−1116	691−1170	900−1390	770−1150	1019−1137
	viscosity (μ_l[b] $\times 10^3$; Pa·s]	0.68−66	0.63−25	1−9	0.55−14	0.9−9.3
	surface tension (σ_l[c] $\times 10^3$; N/m)	10.6−77	10.6−75.6	26.7−77.7	25.5−73	53−61
	mass diffusivity (D_l[d] $\times 10^{11}$; m^2/s)		4.76−979		8.5−329	37−76
gas properties	density (ρ_g;[e] kg/m^3)	1.12−57.5	0.163−36.76	1.12−1.6	0.09−38.17	1.13−103.2
	viscosity (μ_g[f] $\times 10^3$; Pa·s]	1.5×10^{-2}−2×10^{-2}	0.8×10^{-2}−1.8×10^{-2}	1.7×10^{-2}−1.8×10^{-2}	0.93×10^{-2}−1.8×10^{-2}	1.7×10^{-2}−1.9×10^{-2}
	mass diffusivity (D_g[g] $\times 10^6$; m^2/s)			6.11−16		

a_{gl} [m^2/m^3] = 23.4−10746 $k_l a$ [s^{-1}] = 4.245×10^{-4}−7 $k_g a$ [s^{-1}] = 8.8×10^{-3}−6.94 $\eta_e k_{ls}$ [m s^{-1}] = 4.26×10^{-7}−5.9×10^{-4} $\eta_e k_{lw}$ [m s^{-1}] = 4.5×10^{-8}−1.9×10^{-4}

liquids: H_2O, $H_2O + C_6H_6$, H_2O + NaOH [0.1−2 N], $H_2O + Na_2SO_3$ [0.8 M], $H_2O + Na_2SO_4$ [1 M], $H_2O + Na_2SO_4$ [0.5 M] + Co^{2+}, $H_2O + Na_2SO_4$ [0.8 M] + $CoSO_4$ [5×10^{-4} M], H_2O + NaOH [0.5−2 N] + Na_2SO_4, $H_2O + K_2CO_3$ [0.8−1.3 M] + $KHCO_3$ [0.65−1.2 M], $H_2O + Na_2S_2O_3$, H_2O + MEA [0.25−0.33 M], H_2O + DEA [1.5−2 M], H_2O + DIPA [2.4 M], H_2O + DEA [1.5 M] + ETG [20−40%], H_2O + 40% $CaCl_2$, H_2O + naphthalene, H_2O + CHA [0.227−1.177 M] + toluene + 10% IPA, H_2O + EtOH + MEA [0.392 M], H_2O + EtOH + DEA [0.0435−0.875 M], H_2O + ETG + DEA [0.045−1.88 M], ETG + MEA, EtOH + MEA [0.2−0.7 M], EtOH + DEA [0.6−0.8 M], IPA + toluene + CHA [0.1−0.7 M], toluene + 10% IPA + DIPA, *p*-xylene + 10% *i*-PrOH + CHA, *n*-C_4H_9OH + MEA, cumene, H_2O + 0.1% CMC, H_2O + 0.5% CMC, H_2O + 1.0% CMC, H_2O saturated with O_2

gases: He, H_2, air, air +CO_2, air + SO_2, air + O_2, humidified air, $N_2 + CO_2$, $N_2 + O_2$, CO_2

packing shape: spheres, cylinders, extrudates, Raschig and Pall rings, Intalox, Berl saddles

packing material: glass, ceramic, porous alumina, carbon, stainless steel, PE, PP, PVC, CuO−ZnO catalyst, benzoic acid, naphthalene

[a] + for wettable and − for nonwettable. [b] Common liquids;[160] mixtures (the Grunberg and Nissan method[158]). [c] The Macleod and Sugden method;[158] *International Critical Tables*.[159] [d] The Wilke and Chang method.[158] [e] Ideal gas law (≤0.1 MPa), if ≥ 0.1 MPa.[157] [f] Pure gases;[157] mixed gases (the Wilke method[158]). [g] The Takahashi method.[158]

Table 2. Intervals of Operating Conditions for the Mass-Transfer Database in the Upflow Mode

category	properties	a_{gl} range	$k_l a$ range	$\eta_e k_{ls}$ range	$\eta_e k_{lw}$ range
operating conditions	pressure (P; MPa)	0.1−6.4	0.1−1.38	0.1	0
	temperature (T; K)	293−298	293−433	298−303	298
	superficial velocity ($v_{sl} \times 10^2$; m/s)	1×10^{-2}−11.2	4.7×10^{-2}−6	4.5×10^{-2}−25.4	1−8
	superficial velocity ($v_{sg} \times 10^2$; m/s)	0.5−196.5	0.175−221	0.125−110	7−45
	v_{sg}/v_{sl}	0.266−1912	0.085−2103	7×10^{-3}−394	0.98−44.4
packing and bed properties	particle diameter ($d_p \times 10^3$; m)	1.16−34.7	0.5−6	0.5−10	1
	bed porosity (ϵ)	0.34−0.925	0.34−0.463	0.33−0.46	0.4
	bed specific surface area (a_t; m^{-1})	297−7634	590−7634	366−6240	1162
	sphericity factor (ϕ)	0.187−1	0.87−1	0.87−1	1
	material wettability[a]	+	+	+	+
	packed bed height (H; m)	0.35−2	0.1−2	0.01−1.54	0.56
	column diameter ($d_c \times 10^2$; m)	4.5−15.6	2.5−9.4	2.6−12.74	2.5
liquid properties	density (ρ_l;[b] kg/m^3)	1000−1113	813−1192	1000−1021	1006
	viscosity (μ_l[b] $\times 10^3$; Pa·s]	0.9−18	0.9−23.5	0.9−1	1
	surface tension (σ_l[c] $\times 10^3$; N/m)	40−75	13−72	55−72	54
	mass diffusivity (D_l[d] $\times 10^{11}$; m^2/s)		11.6−26	70−94	70
gas properties	density (ρ_g;[e] kg/m^3)	1.21−72.1	0.22−17.82	1.15−1.22	1.14
	viscosity (μ_g[f] $\times 10^3$; Pa·s]	1.7×10^{-2}−1.8×10^{-2}	1.1×10^{-2}−2.06×10^{-2}	1.6×10^{-2}−1.75×10^{-2}	1.7×10^{-2}
	mass diffusivity (D_g[g] $\times 10^6$; m^2/s)				

a_{gl} [m^2/m^3] = 44−1970 $k_l a$ [s^{-1}] = 2.9×10^{-3}−2.73 $\eta_e k_{ls}$ [m s^{-1}] = 5.33×10^{-6}−2.35×10^{-4} $\eta_e k_{lw}$ [m s^{-1}] = 1.9×10^{-5}−7.9×10^{-5}

liquids: H_2O, H_2O + NaOH [0.1−2 N], H_2O + Na_2SO_3 [0.4 M], H_2O + Na_2SO_4 [0.8 M], H_2O + Na_2SO_4 [0.4 M] + Co^{2+}, H_2O + Na_2SO_4 [0.8 M] + $CoSO_4$ [5×10^{-4} M], H_2O + NaOH [0.5−2 N] + Na_2SO_4, H_2O + N_2H_4 [0.04 M] + Na_2SO_4 [0.8 M] + $CoSO_4$ [5×10^{-4} M], H_2O + DEA [1.5−2 M], H_2O + DEA [1.5 M] + ETG [40−68%], H_2O + ETG [40−68%], H_2O + 1% CMC, cyclododecatriene, H_2O + glycerine (30−60%), H_2O saturated with O_2

gases: H_2, air, air + CO_2, air + O_2, N_2 + CO_2, N_2 + O_2, CO_2

packing shape: spheres, cylinders, cylindrical screen, plastic tri-Packs

packing material: glass, ceramic, stainless steel, CuO−ZnO catalyst, benzoic acid, naphthalene, unglazed ceramic, porous alumina

[a] + for wettable and − for nonwettable. [b] Common liquids;[160] mixtures (the Grunberg and Nissan method[158]). [c] The Macleod and Sugden method;[158] *International Critical Tables*.[159] [d] The Wilke and Chang method.[158] [e] Ideal gas law (≤0.1 MPa), if ≥ 0.1 MPa.[157] [f] Pure gases;[157] mixed gases (the Wilke method[158]). [g] The Takahashi method.[158]

published over the past 40 years on the topic of heat and mass transfer in cocurrent downflow and cocurrent upflow packed-bed reactors.

Mass Transfer. (a) Trickle Bed (Cocurrent Downflow). A comprehensive database of over 4000 experimental measurements is first built and then used to develop the new mass-transfer correlations. It is a compilation of data from 65 references relevant to studies on gas−liquid mass transfer and from 28 sources dealing with liquid−solid mass-transfer coefficient measurements. The mass-transfer database corresponds to a summation of 902 volumetric liquid-film ($k_l a$),[10−40] 498 volumetric gas-film mass-transfer coefficients ($k_g a$),[10,17,20,22,41−45] 1484 gas−liquid interfacial areas (a_{gl}),[10,13,20,21,24,26−30,33,41,46−66] 899 liquid−solid mass-transfer coefficients ($\eta_e k_{ls}$),[16,17,23,35,67−89] and 234 liquid−wall mass-transfer coefficients ($\eta_e k_{lw}$).[90−96] Table 1 offers a synthetic summary of these databases. The constructed repository is elaborate and offers an extensive coverage of the trickle-bed operation: (i) more than 80 packings differing in size and shape and 35 column diameters; (ii) atmospheric and high-pressure conditions; (iii) coalescing, noncoalescing, Newtonian, power-law pseudoplastic aqueous and organic, pure, and mixed liquids; (iv) partially ($a_{gl} < a_t$, $\eta_e < 1$) and fully wetted beds ($a_{gl} \geq a_t$, $\eta_e = 1$); (v) various low and high interaction regimes: trickle, pulse, bubble, and dispersed bubble flows and foaming and foaming−pulsing flows.

(b) Packed Bubble Column (Cocurrent Upflow). In comparison with trickle beds, studies on packed bubble columns are less numerous. The thus-constructed mass-transfer database consists of only 1191 measurements for the various parameters (Table 2): 9 sources report liquid−solid mass-transfer coefficients and 15 others are relevant to volumetric liquid-side mass-transfer coefficients and gas−liquid interfacial areas. No work is reported about volumetric gas-side mass-transfer coefficients. The database corresponds to the summation of 499 data on a_{gl},[25,97−103] 439 data on $k_l a$,[17,97,98,100,101,104−110] 230 on $\eta_e k_{ls}$,[17,67,87,89,111−116] and 23 on $\eta_e k_{lw}$.[117] It encompasses 27 different packings and 12 column diameters. The explored conditions cover the bubble and dispersed bubble-flow regimes, as well as the pulse-flow and the spray-flow regimes.

Heat Transfer. (a) Trickle Bed. There are three key heat-transfer characteristics that have been culled from 17 references: the effective radial thermal conductivity, λ_e (376 data[118−127]), the wall heat-transfer coefficient, h_w (507 data[33,119,124−126,128,129]), and the particle-to-fluid heat-transfer coefficient, h_p (379 data[70,130−132]). The 1262 heat-transfer measurements are obtained for 12 packings and 9 column diameters using aqueous and organic liquids in both the low and high interaction regimes (Table 3).

(b) Packed Bubble Column. Unlike trickle beds, studies on the heat transfer in packed bubble columns are scantier. Because of higher liquid holdups, packed bubble columns offer better thermal controllability. Few studies are realized using the same vessel in upward and downward modes so that heat-transfer performances are sometimes compared directly.[119,125] The two characteristics that have been reported in the literature are the effective radial thermal conductivity (295 data[119,125,133−137]) and the wall heat-transfer coefficient (488 data[109,119,125,133,136]). The data collected concerns seven different packings, four column diameters, and aqueous, organic, coalescent, and foaming liquids (see Table 4 for the other operating conditions). Up until now, no work has been published on the particle-to-fluid heat-transfer coefficient (h_p).

Method for Deriving the Mass- and Heat-Transfer Neural Network Correlations

The method surrounding the application of artificial neural network (ANN) computing and the identification

Table 3. Intervals of Operating Conditions for the Heat-Transfer Database in the Downflow Mode

category	properties	h_w range	h_p range	λ_e range
operating conditions	pressure (P; MPa)	0.1	0.1	0.1
	mean temperature in the bed (K)	287−373	287−298	301−338
	superficial velocity ($v_{sl} \times 10^2$; m/s)	6.21×10^{-2}−13.5	0.2−2.2	6×10^{-2}−5.2
	superficial velocity ($v_{sg} \times 10^2$; m/s)	5.23×10^{-2}−154	0.1−68.11	5.23×10^{-2}−132
	v_{sg}/v_{sl}	0.011−778	0.09−193	0.0117−564.86
packing and bed properties	particle diameter (d_p or $d_p' \times 10^3$; m)	1.77−6.6	1.2−6	2.2−12.9
	bed porosity (ϵ)	0.375−0.446	0.38−0.59	0.375−0.623
	bed specific surface area (a_t; m^{-1})	528−2310	650−2045	279−1663
	sphericity factor (ϕ)	0.818−1	0.59−1	0.472−1
	material wettability[a]	+	+	+
	column diameter ($d_c \times 10^2$; m)	5−10	10−30	5.7−60
	thermal conductivity (λ_s; W/m·K)	0.225−1.38	1.38	0.225−28
liquid properties	density (ρ_l;[b] kg/m^3)	778−1109	1000	980−997
	viscosity (μ_l[b] $\times 10^3$; Pa·s)	0.275−15.3	1	0.422−0.8
	surface tension (σ_l[c] $\times 10^3$; N/m)	25−72.5	72	63−72.5
	heat capacity (C_{pl}; J/kg/K)	1730−4180	4180	4066−4180
	thermal conductivity (λ_l; W/m·K)	0.12−0.68	0.604	0.608−0.658
gas properties	density (ρ_g; kg/m^3)	0.95−4.518	1.19−1.21	1.05−1.165
	viscosity ($\mu_g \times 10^3$; Pa·s)	1.75×10^{-2}−2.18×10^{-2}	1.71×10^{-2}−1.75×10^{-2}	1.75×10^{-2}−2.03×10^{-2}
	heat capacity (C_{pg}; J/kg/K)	1006−1041	1006	1006−1041
	thermal conductivity (λ_g; W/m·K)	0.0256−0.0313	0.0256	0.0256−0.0289

h_w [W/m^2·K] = 83.3−8481.9 h_p [W/m^2·K] = 1484−17441 λ_e [W/m·K] = 2.72−152

liquids: H_2O, C_6H_{12}, kerosene, gasoil, ETG, H_2O + [0.02%] pentanol
gases: air, N_2
packing shape: spheres, Raschig rings, cylinders
packing material: glass, ceramic, alumina, TCC, spheralite, unkown catalyst

[a] + for wettable and − for nonwettable. [b] Common liquids;[160] mixtures (the Grunberg and Nissan method[158]). [c] The Macleod and Sugden method;[158] *International Critical Tables.*[159]

Table 4. Intervals of Operating Conditions for the Heat-Transfer Database in the Upflow Mode

category	properties	h_w range	λ_e range
operating conditions	pressure (P; MPa)	0.1−0.6	0.1
	mean temperature in the bed (K)	295−433	295−338
	superficial velocity ($v_{sl} \times 10^2$; m/s)	3.21×10^{-2}−2.74	5×10^{-2}−2.66
	superficial velocity ($v_{sg} \times 10^2$; m/s)	1×10^{-3}−113	1×10^{-2}−67
	v_{sg}/v_{sl}	9.6×10^{-4}−2463	9.6×10^{-4}−331
packing and bed properties	particle diameter (d_p or $d_p' \times 10^3$; m)	1− 6.6	2−6.6
	bed porosity (ϵ)	0.36−0.44	0.37−0.4
	bed specific surface area (a_t; m^{-1})	545−3360	545−1860
	sphericity factor (ϕ)	0.87−1	1
	material wettability[a]	+	+
	column diameter ($d_c \times 10^2$; m)	2.6−10	5−10
	thermal conductivity (λ_s; W/m·K)	0.225−1.38	1.15−1.38
liquid properties	density (ρ_l;[b] kg/m^3)	813−1062	980−1062
	viscosity (μ_l[b] $\times 10^3$; Pa·s)	0.3−4	0.422−1.2
	surface tension (σ_l[c] $\times 10^3$; N/m)	32−72.5	32−72.5
	heat capacity (C_{pl}; J/kg/K)	1910−4180	3220−4180
	thermal conductivity (λ_l; W/m·K)	0.11−0.68	0.38−0.658
gas properties	density (ρ_g; kg/m^3)	0.95−1.56	1.05−1.56
	viscosity ($\mu_g \times 10^3$; Pa·s)	0.9×10^{-2}−2.14×10^{-2}	1.75×10^{-2}−2.03×10^{-2}
	heat capacity (C_{pg}; J/kg/K)	1006−1041	1008−1041
	thermal conductivity (λ_g; W/m·K)	0.0256−0.0313	0.0256−0.0289

h_w [W/m^2·K] = 130−11222 λ_e [W/m·K] = 1.5−126.8

liquids: H_2O, H_2O + [1.5%] pentanol, cyclododecatriene, H_2O + [40−60%] ETG
gases: air, N_2
packing shape: spheres, cylinders
packing material: glass, ceramic, alumina

[a] + for wettable and − for nonwettable. [b] Common liquids;[160] mixtures (the Grunberg and Nissan method[158]). [c] The Macleod and Sugden method;[158] *International Critical Tables.*[159]

of the best set of dimensionless groups to be involved in the correlations have been addressed elsewhere.[138−140] Briefly, several dimensionless groups are generated by clustering the dimensional variables having a potential impact on the mass- and heat-transfer parameters to form dimensionless combinations with the objective of forming the smallest assortment of dimensionless groups best correlated to the heat- and mass-transfer parameters.

The optimal assortment of dimensionless groups intervening in the neural network correlations is selected using a trial-and-error procedure and must fulfill the following criteria:

(i) The ANN correlations must contain a minimum number of dimensionless groups.

(ii) The optimal set of groups must yield the best match of the output, i.e., minimal absolute average relative error (AARE) and standard deviation (σ).

(iii) The neural network architecture must be of minimal complexity, i.e., the least number of hidden

Table 5. Inputs, Output, and Connectivity Weights of the Trickle Bed k_la Correlation

Normalized output

$$\Gamma_j = \frac{1}{1+\exp\left(-\sum_{i=1}^{8}\omega_{ij}\Omega_i\right)} \quad (1)$$

$$\Psi = \frac{1}{1+\exp\left(-\sum_{j=1}^{9}\omega_j\Gamma_j\right)} \quad (2)$$

$$\Psi = \frac{\log\left(\frac{Sh_\ell}{4.73\times10^{-3}}\right)}{7.305}$$

$1 \le J \le 8 \quad \Gamma_9 = 1$

where $Sh_\ell = \dfrac{k_\ell a d_h^2}{D_\ell}$

Normalized inputs

$$\Omega_1 = \frac{\log\left(\frac{St_{g\ell}}{1.075\times10^{-5}}\right)}{4.86} \quad \Omega_2 = \frac{\log\left(\frac{We_\ell}{2.92\times10^{-11}}\right)}{11.099} \quad \Omega_3 = \frac{\log\left(\frac{Re_g}{0.0124}\right)}{5.6764} \quad \Omega_4 = \frac{\log\left(\frac{Ca_{g\ell}}{4.53\times10^{-7}}\right)}{3.3901} \quad \Omega_5 = \frac{\log\left(\frac{(d_c/H)}{0.019}\right)}{1.718} \quad \Omega_6 = \frac{\log\left(\frac{S_b}{2.528}\right)}{1.978}$$

$$\Omega_7 = \frac{\log\left(\frac{Sc_\ell}{102.7}\right)}{3.6775} \quad \Omega_8 = 1$$

$$St_{g\ell} = \frac{(v_{s\ell}+v_{sg})\mu_\ell}{g\rho_\ell d_p^2} \quad We_\ell = \frac{\rho_\ell v_{s\ell}^2 d_p}{\sigma_\ell} \quad Re_g = \frac{\rho_g v_{sg} d_p}{\mu_g} \quad Ca_{g\ell} = \frac{\mu_g(v_{sg}+v_{s\ell})}{\sigma_\ell} \quad Sc_\ell = \frac{\mu_\ell}{\rho_\ell D_\ell} \quad S_b = \frac{a_s d_h}{1-\varepsilon}$$

Domain of applicability

$1.75\times10^{-5} \le St_{g\ell} \le 0.7788 \quad 2.92\times10^{-11} \le We_\ell \le 3.672 \quad 0.0124 \le Re_g \le 5882$

$4.53\times10^{-7} \le Ca_{g\ell} \le 1.15\times10^{-3} \quad 0.019 \le d_c/H \le 1 \quad 2.52 \le S_b \le 240 \quad 102.7 \le Sc_\ell \le 4.9\times10^5$

Connectivity weights

ω_{ij}	1	2	3	4	5	6	7	8
1	8.67806	-1.9267	22.8877	3.94213	-2.45559	20.79	-20.0723	15.5828
2	-5.99962	2.29352	-1.98418	-7.11879	1.11252	-8.68117	-11.5915	3.2374
3	-9.52999	0.237931	-20.0403	-8.24774	12.5499	16.1034	-6.06239	-0.328687
4	-0.534556	2.32783	-1.04558	-3.64856	-1.66543	-14.3247	11.2905	-12.9761
5	5.27202	0.462239	-7.18071	0.425952	3.27321	-37.6903	-1.57758	0.407462
6	-42.7277	0.133048	6.38769	-2.49272	13.2657	28.5918	-3.32684	-16.4045
7	-4.44135	1.29744	0.578028	0.649584	-13.9821	-14.1898	3.92092	4.58479
8	1.70278	-5.12514	-7.95968	-5.36287	-2.14088	5.68573	11.3201	-3.95478

ω_j	1	2	3	4	5	6	7	8	9
	-2.86352	14.6706	-10.6858	-2.66679	2.05524	1.16672	0.814109	3.00521	-3.6439

Table 6. Inputs, Output, and Connectivity Weights of the Trickle Bed k_ga Correlation

Normalized output

$$\Gamma_j = \frac{1}{1+\exp\left(-\sum_{i=1}^{7}\omega_{ij}\Omega_i\right)} \quad (1)$$

$$\Psi = \frac{1}{1+\exp\left(-\sum_{j=1}^{8}\omega_j\Gamma_j\right)} \quad (2)$$

$$\Psi = \frac{\log\left(\frac{Sh_g}{1.487\times10^{-4}}\right)}{6.73222}$$

$1 \le J \le 7 \quad \Gamma_8 = 1$

where $Sh_g = \dfrac{k_g a d_h^2}{D_g}$

Normalized inputs

$$\Omega_1 = \frac{\log\left(\frac{Re_\ell}{0.2109}\right)}{2.68185} \quad \Omega_2 = \frac{\log\left(\frac{St_\ell}{6.188\times10^{-7}}\right)}{3.46399} \quad \Omega_3 = \frac{\log\left(\frac{Re_g}{0.1439}\right)}{3.99819} \quad \Omega_4 = \frac{\log\left(\frac{Fr_g}{5.126\times10^{-4}}\right)}{4.95396} \quad \Omega_5 = \frac{\log\left(\frac{Sc_g}{0.0269}\right)}{0.46492}$$

$$\Omega_6 = \frac{\log\left(\frac{S_b}{1.717}\right)}{2.10461} \quad \Omega_7 = 1$$

$$Re_\alpha = \frac{\rho_\alpha v_{s\alpha} d_p}{\mu_\alpha} \quad St_\ell = \frac{v_{s\ell}\mu_\ell}{g\rho_\ell d_p^2} \quad Fr_g = \frac{v_{sg}^2}{g d_p} \quad Sc_g = \frac{\mu_g}{\rho_g D_g} \quad S_b = \frac{a_s d_h}{1-\varepsilon}$$

Domain of applicability

$0.21 \le Re_\ell \le 101.387 \quad 6.19\times10^{-7} \le St_\ell \le 1.8\times10^{-3} \quad 0.144 \le Re_g \le 1433$

$5.12\times10^{-4} \le Fr_g \le 46.11 \quad 0.807 \le Sc_g \le 2.353 \quad 1.717 \le S_b \le 218.5$

Connectivity weights

ω_{ij}	1	2	3	4	5	6	7
1	0.45064	-1.26161	-1.1481	-0.45994	-3.52602	-1.20776	-0.19002
2	-1.03878	-4.48762	4.65502	0.337379	3.66946	2.06886	0.336456
3	-1.40158	4.22143	-5.13156	1.80365	-8.83908	0.0870964	6.00514
4	-0.455043	3.74466	-0.822598	1.35251	-6.04263	0.56266	-4.2856
5	-2.27804	-1.16601	6.6835	-1.72779	-0.179682	1.87231	1.86911
6	-1.62934	6.36605	-10.5601	0.109652	-6.71277	-0.259201	1.91717
7	4.63341	-0.507541	2.00459	-1.27904	-0.281331	-1.43813	0.885562

ω_j	1	2	3	4	5	6	7	8
	-8.94301	-0.44023	0.835614	3.73	-6.28843	-3.89636	3.90037	4.11065

neurons giving the smallest errors on both the developmental or training data set (70% of the database) and the generalization data set (the 30% hidden instances).

(iv) The optimal ANN correlations must preserve, at least within the database domain, the expected behavior of the output in accordance with all known aspects documented in the literature about the process physics.

Neural Network Correlations. The three-layer neural network correlations are designed by means of the NNfit software.[141] The structure of the correlations is described by the recurrent equations (1) and (2) from Tables 5−11. In these equations, $\mathbf{\Omega}$ and $\mathbf{\Gamma}$ define the input and hidden-layer vectors and Γ_{J+1} and Ω_{I+1} are bias constants set to 1, ω_{ij} and ω_j are connectivity weights, and J is the number of nodes in the hidden layer. Equations 1 and 2 correlate the neural network normalized output, Ψ, to the normalized input vector $\mathbf{\Omega}$. The weights are adjusted by minimizing, via the quasi-Newton−Broyden−Fletcher−Goldfarb−Shanno algorithm,[142] a quadratic training error on a learning data set. A good measure for robustness of well-trained neural network correlations is decided based on

Table 7. Inputs, Output, and Connectivity Weights of the Trickle-Bed Gas−Liquid Interfacial Area Correlation

Normalized output

$$\Gamma_j = \frac{1}{1+\exp\left(-\sum_{i=1}^{7}\omega_{ij}\Omega_i\right)} \quad (1)$$

$$\Psi = \frac{1}{1+\exp\left(-\sum_{j=1}^{11}\omega_j\Gamma_j\right)} \quad (2)$$

$$\Psi = \frac{\log\left(\frac{a_{g\ell}d_h/(1-\varepsilon)}{0.00984}\right)}{4.74815}$$

$1 \le J \le 10 \qquad \Gamma_{11} = 1$

Normalized inputs

$$\Omega_1 = \frac{\log\left(\frac{Re_\ell}{0.0879}\right)}{4.5184} \quad \Omega_2 = \frac{\log\left(\frac{Re_g}{1.77}\right)}{3.5472} \quad \Omega_3 = \frac{\log\left(\frac{We_g}{3.55\times10^{-6}}\right)}{6.28609} \quad \Omega_4 = \frac{\log\left(\frac{Fr_\ell}{9.67\times10^{-6}}\right)}{4.97836} \quad \Omega_5 = \frac{\log\left(\frac{Eo_\ell}{0.0269}\right)}{3.77164} \quad \Omega_6 = \frac{\log\left(\frac{S_b}{1.63}\right)}{2.211106}$$

$\Omega_7 = 1$

$$\text{where: } Re_\alpha = \frac{\rho_\alpha v_{s\alpha} d_p}{\mu_\alpha} \quad We_g = \frac{\rho_g v_{sg}^2 d_p}{\sigma_\ell} \quad Fr_\ell = \frac{v_{s\ell}^2}{g d_p} \quad Eo_\ell = \frac{\rho_\ell g d_p^2 \phi^2 \varepsilon^2}{\sigma_\ell (1-\varepsilon)^2} \quad S_b = \frac{a_s d_h}{1-\varepsilon}$$

Domain of applicability

$8.79\times10^{-2} \le Re_\ell \le 2900 \quad 1.77 \le Re_g \le 6240 \quad 3.55\times10^{-6} \le We_g \le 6.86$

$9.67\times10^{-6} \le Fr_\ell \le 0.92 \quad 2.69\times10^{-2} \le Eo_\ell \le 159 \quad 1.63 \le S_b \le 265$

Connectivity weights

ω_{ij}	1	2	3	4	5	6	7	8	9	10
1	10.2614	16.3369	-0.113971	6.32291	-12.7714	3.89916	6.00709	-13.6436	-14.6674	7.38205
2	-5.5053	-12.811	-4.36891	-59.1211	12.098	17.8136	17.1643	-14.0496	-13.8192	11.3694
3	4.75942	10.6384	14.6109	52.3525	-9.54826	-12.0335	-19.5205	12.3321	14.3032	-9.5317
4	-6.23624	-8.34824	4.58873	5.40628	7.65951	0.642268	-7.00092	8.28606	9.53729	-3.62453
5	-29.7851	-7.74647	2.96664	-1.31615	5.27775	0.804716	0.425372	18.383	16.9044	8.17504
6	-0.246207	3.45393	10.3755	3.06225	-1.02769	4.08478	-7.49868	-6.6127	6.50537	42.6939
7	26.8609	-1.34963	-3.74434	-10.6391	1.08334	2.79787	9.5993	1.73713	-1.05848	1.08616

ω_j	1	2	3	4	5	6	7	8	9	10	11
	-6.58534	3.12133	-1.87488	-1.0456	4.2625	33.0491	-3.15831	-11.0199	8.43652	-19.8385	-3.42145

Table 8. Inputs, Output, and Connectivity Weights of the Trickle-Bed $\eta_e k_{ls}$ Correlation

Normalized output

$$\Gamma_j = \frac{1}{1+\exp\left(-\sum_{i=1}^{6}\omega_{ij}\Omega_i\right)} \quad (1)$$

$$\Psi = \frac{1}{1+\exp\left(-\sum_{j=1}^{9}\omega_j\Gamma_j\right)} \quad (2)$$

$$\Psi = \frac{\log\left(\frac{\eta_e Sh_{\ell s}}{0.43495}\right)}{3.4955}$$

$1 \le J \le 8 \qquad \Gamma_9 = 1$

$$\text{where: } \eta_e Sh_{\ell s} = \frac{\eta_e k_{\ell s} d'_p}{D_\ell}$$

Normalized inputs

$$\Omega_1 = \frac{\log\left(\frac{Re_{g\ell}}{1.816}\right)}{4.39} \quad \Omega_2 = \frac{\log\left(\frac{St_\ell}{3.75\times10^{-7}}\right)}{4.15864} \quad \Omega_3 = \frac{\log\left(\frac{Ga_\ell}{519}\right)}{4.9757} \quad \Omega_4 = \frac{\log\left(\frac{Sc_\ell}{168.3}\right)}{2.386} \quad \Omega_5 = \frac{\log\left(\frac{S_b}{2.48}\right)}{0.9979} \quad \Omega_6 = 1$$

$$Re_{g\ell} = \frac{\rho_\ell (v_{s\ell}+v_{sg}) d'_p}{\mu_\ell (1-\varepsilon)} \quad St_\ell = \frac{v_{s\ell}\mu_\ell}{g\rho_\ell d'^2_p} \quad Ga_L = \frac{d'^2_p \rho_\ell^2 g \varepsilon^3}{\mu_\ell^2 (1-\varepsilon)^3} \quad Sc_\ell = \frac{\mu_\ell}{D_\ell \rho_\ell} \quad S_b = \frac{a_s d'_h}{1-\varepsilon}$$

Domain of applicability

$1.816 \le Re_{g\ell} \le 44587.5 \quad 3.75\times10^{-7} \le St_\ell \le 5.4\times103 \quad 519 \le Ga_\ell \le 4.908\times10^7$

$168 \le Sc_\ell \le 40921 \quad 2.48 \le S_b \le 24.7$

Connectivity weights

ω_{ij}	1	2	3	4	5	6	7	8
1	0.734333	0.554249	0.154199	-0.525451	0.988983	0.444113	3.2808	0.630407
2	3.29609	-2.0172	0.520189	0.425466	5.49777	2.37516	8.32124	-1.95846
3	41.1905	19.5613	1.06197	-0.169243	64.607	41.2869	4.39906	20.4279
4	12.3901	8.8862	-1.5845	8.32964	12.6881	15.0348	13.854	9.19531
5	-1.37005	-0.636883	-0.712226	1.45765	-4.97142	-0.825238	0.638706	-0.102436
6	-28.3227	-12.3225	1.04563	0.886363	-39.9893	-29.4614	-15.2693	-12.9275

ω_j	1	2	3	4	5	6	7	8	9
	-42.4149	-43.3134	22.5013	16.0774	9.82588	32.9471	3.34152	42.207	-32.1402

the generalization error (30% remaining portion). This error must be close to the learning error for input/output instances dissimulated during learning. Tables 5−11 list the fitted weights of each correlation.

The dimensionless groups retained for each of the correlations are as follows:

(a) Trickle Bed.

(i) For Sh_l: Stokes group or viscosity-to-gravity forces ratio (St_{lg}), liquid Weber number (We_l), gas Reynolds number (Re_g), capillarity number or viscosity-to-capillary forces ratio (Ca_{gl}), liquid Schmidt number (Sc_l), bed aspect ratio (d_c/H), and bed correction function (S_b).

(ii) For Sh_g: liquid Reynolds number (Re_l), liquid Stokes number (St_l), Re_g, gas Froude number (Fr_g), Sc_g, and S_b.

(iii) For $a_{gl}d_h/(1-\epsilon)$: Re_l, Re_g, We_g, Fr_l, Eötvös number or gravity-to-capillary forces ratio (Eo_l), and S_b.

(iv) For $\eta_e Sh_{ls}$: mixed Reynolds number (Re_{lg}), St_l, Galileo number or gravity-to-viscosity forces ratio (Ga_l), Sc_l, and S_b.

(v) For $\eta_e k_{lw}$: recommended literature correlation.

(vi) For Nu: Re_l, ratio between gas inertia-to-gas heat conduction and liquid inertia-to-liquid heat conduction ($Pe_{gl} = Pe_g/Pe_l$), We_l, Fr_g, St_l, and particle-to-column diameter ratio (d_p/d_c).

Table 9. Inputs, Output, and Connectivity Weights of the Trickle-Bed h_w Correlation

Normalized output

$$\Gamma_j = \frac{1}{1+\exp\left(-\sum_{i=1}^{7}\omega_{ij}\Omega_i\right)} \quad (1)$$

$$\Psi = \frac{1}{1+\exp\left(-\sum_{j=1}^{6}\omega_j\Gamma_j\right)} \quad (2)$$

$$\Psi = \frac{\log\left(\frac{Nu}{0.43495}\right)}{1.9319}$$

$1 \le J \le 5 \quad \Gamma_6 = 1$

$$\text{where: } Nu = \frac{h_w d_p}{\lambda_\ell}$$

Normalized inputs

$$\Omega_1 = \frac{\log\left(\frac{Re_\ell}{3.76}\right)}{2.5393} \quad \Omega_2 = \frac{\log\left(\frac{Pe_{g\ell}}{7.78\times10^{-5}}\right)}{4.78734} \quad \Omega_3 = \frac{\log\left(\frac{We_\ell}{2.78\times10^{-5}}\right)}{4.79056} \quad \Omega_4 = \frac{\log\left(\frac{Fr_g}{4.65\times10^{-6}}\right)}{7.35465}$$

$$\Omega_5 = \frac{\log\left(\frac{St_\ell}{9.83\times10^{-7}}\right)}{4.1708} \quad \Omega_6 = \frac{\log\left(\frac{d_p/d_c}{0.035}\right)}{0.5149} \quad \Omega_7 = 1$$

$$Re_\ell = \frac{\rho_\ell v_{s\ell} d_p}{\mu_\ell(1-\varepsilon)} \quad Pe_{g\ell} = \frac{\rho_g v_{sg} c_{pg} \lambda_\ell}{\rho_\ell v_{s\ell} c_{p\ell} \lambda_g} \quad We_\ell = \frac{\rho_\ell v_{s\ell}^2 d_p}{\sigma_\ell} \quad Fr_g = \frac{v_{sg}^2}{g d_p} \quad St_\ell = \frac{v_{s\ell}\mu_\ell}{g\rho_\ell d_p^2}$$

Domain of applicability

$3.76 \le Re_\ell \le 1290 \quad 7.786\times10^{-5} \le Pe_{g\ell} \le 4.77 \quad 2.78\times10^{-5} \le We_\ell \le 1.717$

$4.64\times10^{-6} \le Fr_g \le 105 \quad 9.81\times10^{-7} \le St_\ell \le 0.0145 \quad 0.035 \le d_p/d_c \le 0.116$

Connectivity weights

ω_{ij}	1	2	3	4	5
1	-3.33435	-7.74698	-5.23381	-3.14786	-11.3796
2	-0.0811699	-1.36875	-14.8817	3.21093	14.5275
3	9.80518	5.70108	-7.15333	20.558	17.9117
4	1.04392	-21.0441	9.36157	-5.65842	-13.4469
5	-7.2261	21.5877	21.0406	-10.4221	9.66137
6	-1.12961	-21.7535	-10.6273	-1.92344	-14.9289
7	-0.228836	37.8053	10.9253	-7.71048	4.5901

ω_j	1	2	3	4	5	6
	4.40073	1.74866	16.1299	6.16598	-16.7635	-2.87202

Table 10. Inputs, Output, and Connectivity Weights of the Trickle-Bed λ_e Correlation

Normalized output

$$\Gamma_j = \frac{1}{1+\exp\left(-\sum_{i=1}^{7}\omega_{ij}\Omega_i\right)} \quad (1)$$

$$\Psi = \frac{1}{1+\exp\left(-\sum_{j=1}^{5}\omega_j\Gamma_j\right)} \quad (2)$$

$$\Psi = \frac{\log\left(\frac{\lambda_e/\lambda_\ell}{4.129}\right)}{1.78192}$$

$1 \le J \le 4 \quad \Gamma_5 = 1$

Normalized inputs

$$\Omega_1 = \frac{\log\left(\frac{Re_\ell}{9.08}\right)}{1.9344} \quad \Omega_2 = \frac{\log\left(\frac{Fr_g}{4.64\times10^{-6}}\right)}{6.9446} \quad \Omega_3 = \frac{\log\left(\frac{We_\ell}{2.339\times10^{-5}}\right)}{3.9431} \quad \Omega_4 = \frac{\log\left(\frac{Pe_\ell}{15.89}\right)}{2.1105}$$

$$\Omega_5 = \frac{\log\left(\frac{Pe_G}{0.142}\right)}{2.03} \quad \Omega_6 = \frac{\log(Bi/0.199)}{2.11487} \quad \Omega_7 = 1$$

$$Re_\ell = \frac{\rho_\ell v_{s\ell} d_p}{\mu_\ell(1-\varepsilon)} \quad Fr_g = \frac{v_{sg}^2}{g d_p} \quad We_\ell = \frac{\rho_\ell v_{s\ell}^2 d_p}{\sigma_\ell} \quad Pe_\ell = \frac{\rho_\ell v_{s\ell} c_{p\ell} d_p}{\lambda_\ell} \quad Pe_g = \frac{\rho_g v_{sg} c_{pg} d_p}{\lambda_g}$$

$$Bi = \frac{(1-\varepsilon)\lambda_s}{\lambda_\ell}$$

Domain of applicability

$9.08 \le Re_\ell \le 781 \quad 4.64\times10^{-6} \le Fr_g \le 4082 \quad 2.339\times10^{-5} \le We_\ell \le 0205$

$15.89 \le Pe_\ell \le 2049.4 \quad 0.1419 \le Pe_g \le 754.9 \quad 0.199 \le Bi \le 26$

Connectivity weights

ω_{ij}	1	2	3	4
1	0.281371	5.17984	0.323855	32.645
2	-5.31624	8.5468	-15.3767	8.90232
3	-1.11396	-9.96461	-1.47448	-10.118
4	4.63858	6.46109	3.76167	-24.5872
5	2.01861	-8.90981	9.00465	-5.68008
6	-13.9935	-0.64337	-4.42415	-14.6816
7	14.8405	-1.33908	8.58823	5.82917

ω_j	1	2	3	4	5
	8.68581	13.1688	-4.01526	-3.45919	-8.04561

(vii) For λ_e/λ_l: Re_l, Fr_g, We_l, liquid Péclet number (Pe_l), gas Péclet number (Pe_g), and solid-to-liquid thermal conductivity ratio $(1 - \epsilon)\lambda_s/\lambda_l$.

(b) Packed Bubble Column.

(i) For $a_{gl}d_h/(1 - \epsilon)$: Re_l, Re_g, St_l, X_l, We_l, and S_b.

(ii) For Sh_l, $\eta_e Sh_{ls}$, $\eta_e k_{lw}$, Nu, and λ_e/λ_l: recommended literature correlations.

Performance of Mass-Transfer Correlations

Liquid-Side Volumetric Mass-Transfer Coefficient. (a) Trickle Bed. The best $k_l a$ correlations for trickle beds are tested throughout their *valid* ranges as shown in Table 12. As can be seen, the presently developed correlation reduces the prediction error by a factor of 6 compared to the correlation of Wild et al.[143]

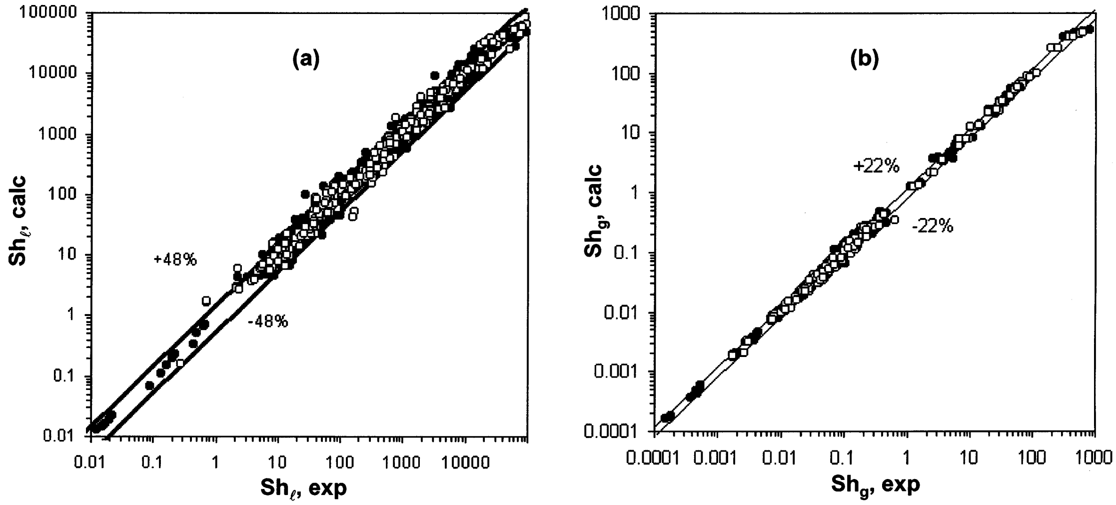

Figure 1. Correlation predictions versus experimental (a) liquid and (b) gas Sherwood numbers in trickle beds: (●) training data set; (○) test data set.

Table 11. Inputs, Output, and Connectivity Weights of the Gas–Liquid Interfacial Area Correlation for Packed Bubble Columns

Normalized output

$$\Gamma_j = \frac{1}{1+\exp\left(-\sum_{i=1}^{7}\omega_{ij}\Omega_i\right)} \quad (1)$$

$$\Psi = \frac{1}{1+\exp\left(-\sum_{j=1}^{5}\omega_j\Gamma_j\right)} = \frac{\log\left(\frac{a_{g\ell}d_h/(1-\varepsilon)}{0.0249}\right)}{4.0228} \quad (2)$$

$1 \le J \le 4 \quad \Gamma_5 = 1$

Normalized inputs

$$\Omega_1 = \frac{\log\left(\frac{Re_\ell}{0.111}\right)}{3.56} \quad \Omega_2 = \frac{\log\left(\frac{Re_g}{0.827}\right)}{3.33763} \quad \Omega_3 = \frac{\log\left(\frac{St_\ell}{5.93\times10^{-7}}\right)}{4.32213} \quad \Omega_4 = \frac{\log\left(\frac{X_\ell}{0.0148}\right)}{3.7818}$$

$$\Omega_5 = \frac{\log\left(\frac{We_\ell}{0.0269}\right)}{3.77164} \quad \Omega_6 = \frac{\log\left(\frac{S_b}{2.27}\right)}{1.8182} \quad \Omega_7 = 1$$

$$Re_\alpha = \frac{\rho_\alpha v_{s\alpha} d_p}{\mu_\alpha} \quad We_\ell = \frac{\rho_\ell v_{s\ell}^2 d_p}{\sigma_\ell} \quad X_\ell = \frac{v_{s\ell}\sqrt{\rho_\ell}}{v_{sg}\sqrt{\rho_g}} \quad St_\ell = \frac{u_\ell \mu_\ell}{g\rho_\ell d_p^2} \quad S_b = \frac{a_s d_h}{1-\varepsilon}$$

Domain of applicability

$0.111 \le Re_\ell \le 406 \quad 0.82 \le Re_g \le 1800 \quad 6.66\times10^{-7} \le We_\ell \le 0.302331$

$0.0148 \le X_\ell \le 90 \quad 5.93\times10^{-7} \le St_\ell \le 0.0124 \quad 2.27 \le S_b \le 149.4$

ANN connectivity weights

ω_{ij}	1	2	3	4
1	1.40907	-1.32567	-0.525531	2.93217
2	5.00698	1.07553	3.18773	4.86236
3	-11.7411	-1.51096	-11.8179	0.731652
4	4.64459	-0.565619	2.31654	3.66307
5	-1.83918	1.24835	1.16605	-8.33033
6	16.9587	-8.86694	-8.44064	-5.19241
7	5.40139	2.21833	7.20486	-1.07939

ω_j	1	2	3	4	5
	11.6726	10.9405	-12.3271	-3.62245	-6.81351

and by a factor of 3.5 compared to that of Turek and Lange.[36] Respective scatters between the neural network predicted values and experimental values for the learning file, the generalization file, and the whole database are also given. As seen in Figure 1a, more than 90% of the 902 k_la data are predicted to fall within the $\pm$2 AARE envelopes, i.e., $\pm$48% error.

(b) Packed Bubble Column. The 439 data on k_la for the packed bubble column database are not so diversified to allow a confident neural network correlation to be developed. Rather we will identify, among the literature correlations, which ones are suited for allowing the best k_la predictions. Only four correlations[98,100,144,145] are available for k_la in packed bubble columns. Among them, the correlation by Takahashi and Alkire[145] is the less general one because it is specific to one single liquid and one particle size. Reiss[144]

Table 12. Performance of Literature and Present Correlations To Predict the k_la Mass-Transfer Coefficient

	statistical parameter		
correlation	no. of data	AARE (%)	σ (%)
	Trickle Bed		
Turek and Lange[36,a]	200	85.0	19.0
Wild et al.[143]	902	145	234
ANN, training file	632	23.5	22.6
ANN, test file	270	24.8	24.3
ANN, correlation	902	24.0	23.0
	Packed Bubble Column		
Saada[98]	439	82	32
	122[b]	58	43
Specchia et al.[100]	439	>500	>500

[a] Applicable only for low gas and liquid Reynolds number (200 data). [b] Data in the validity range of the correlation.

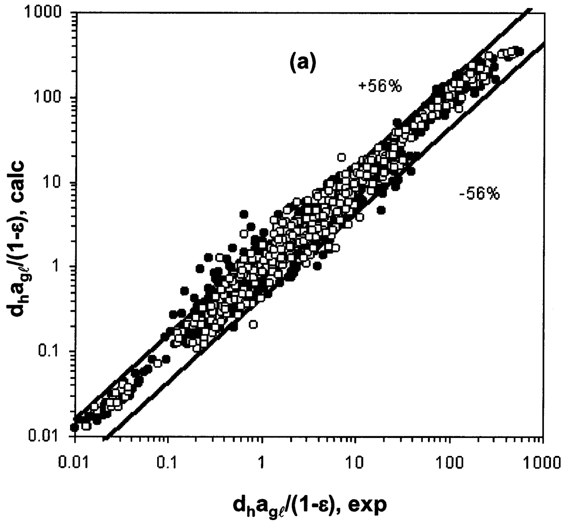

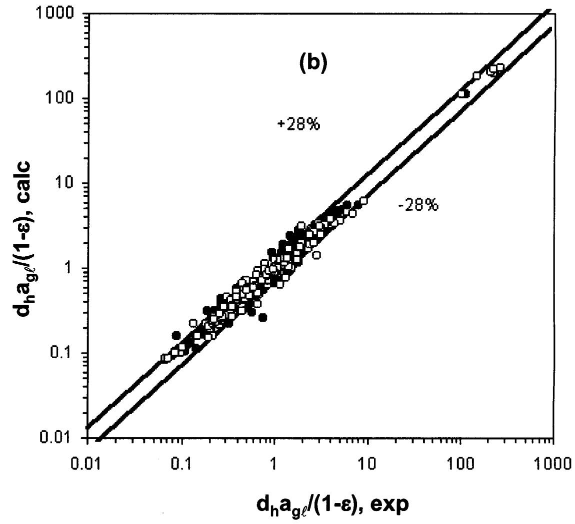

Figure 2. Correlation predictions versus experimental dimensionless interfacial areas in (a) trickle beds and (b) packed bubble columns: (●) training data set; (○) test data set.

Table 13. Performance of Literature and Present Correlations To Predict the k_ga Mass-Transfer Coefficient

correlation	statistical parameter: no. of data	AARE (%)	σ (%)
	Trickle Bed		
Wild et al.[143]	498	60.0	62.5
	318[a]	42.4	34.3
Yaici[43]	498	40.0	49.6
	318[a]	26.0	19.5
ANN, training file	349	10.6	8.7
ANN, test file	149	11.9	9.0
ANN, correlation	498	11.0	8.8

[a] Data in the validity range of the correlation.

Table 14. Performance of Literature and Present Correlations To Predict the Gas−Liquid Interfacial Area a_{gl}

correlation	statistical parameter: no. of data	AARE (%)	σ (%)
	Trickle Bed		
Wild et al.[143]	1471	110	199
	929[a]	82.2	140
Ratnam et al.[60]	1486	82.5	129
	370[a]	42.2	30.8
ANN, training file	1039	28.0	34.5
ANN, test file	444	28.0	28.0
ANN, correlation	1483	28.0	33.0
	Packed Bubble Column		
Lara-Marquez[97]	495	231	367
	227[a]	36.6	50.5
ANN, training file	347	13.6	12.9
ANN, test file	148	15.1	13.7
ANN, correlation	495	14.0	13.2

[a] Data in the validity range of the correlation.

expressed k_la proportionally to the square root of the energy dissipated in the liquid phase. Specchia et al.,[100] by comparing mass transfer in upflow and downflow, found that, because of a higher energy dissipation in the liquid phase, k_la and a_{gl} are greater in packed bubble columns than in trickle beds. Their k_la correlation requires the two-phase pressure drop as an input and is estimated from the Turpin and Huntington[146] correlation as they suggested.[100] As can be seen from Table 12, this approach is not very reliable because the estimation of the pressure drop by this correlation is not very accurate. Saada[98] related k_la to the liquid and gas Reynolds numbers and to the d_p/d_c ratio via a power-law equation that contains flow regime dependent parameters. The predictions by this correlation for conditions falling into the valid range are acceptable; see Table 12. This correlation appears to be the most appropriate for k_la estimation in packed bubble columns.

Gas-Side Volumetric Mass-Transfer Coefficient. Trickle Bed. Predictions of k_ga using the two correlations available in the literature[43,143] and the presently derived correlation (Table 6) are compared in Table 13. From Figure 1b, 92% of the measured gas-side mass-transfer coefficients are predicted within a ±2 AARE limit of ±22%. It is worth mentioning that not a single study exists in the literature about k_ga measurements in packed bubble columns.

Gas−Liquid Interfacial Area. (a) Trickle Bed. Several correlations are proposed in the literature to predict gas−liquid interfacial areas in trickle-bed reactors.[24,25,48,49,51,60,143] Table 14 illustrates the performance of the two best literature correlations[60,143] and the one proposed in this work. The latter improves a_{gl} predictions by a factor of 2.9, and 96% of the experimental data fall within the envelopes of ±56% (±2 AARE) as shown in Figure 2a.

(b) Packed Bubble Column. For this configuration, very few correlations exist in the literature to estimate a_{gl}.[97,99,100] In Table 14, the best among them[97] exhibits an excessively inflated error when compared over the whole database to the present neural network correlation. It is worth mentioning that Lara-Marquez[97] uses the two-phase pressure drop as an input for his correlation. This may cause such inflation in error due to inaccuracies in pressure drop estimations especially outside the valid range of the interfacial area correlation; see Table 14. The parity plot of the predicted versus measured a_{gl} values by the new correlation is shown in Figure 2b.

Liquid−Solid Mass-Transfer Coefficient. (a) Trickle Bed. The literature correlations for liquid-particle mass-transfer coefficients are of two types: (1) those involving the fluid interstitial/superficial Reynolds numbers[70,71,77,78,83−85,89,147,148] (2) and those using the Kolmogorov group.[81,83−85]

Table 15. Performance of Literature and Present Correlations To Predict the Liquid−Solid Mass-Transfer Coefficient

ref	author's correlation within the database valid range			author's correlation over the whole database	
	no. of data	AARE (%)	σ (%)	AARE (%)	σ (%)
Trickle Bed					
Chou et al.[71]	17	4.9	3.3	>300	>300
Hirose et al.[77]	122	33	36	137	>300
Dharwadkar and Sylvester[147]	225	18	14	134	>300
Yoshikawa et al.[89,a]	31	19	41	118	>300
Ruether et al.[84]					
all flow regimes (eqs 17−19[b])	35	19.5	16	267	>300
pulse flow (eq 11[b])	18	25	9	>300	>300
Rao and Drinkenburg[83]					
trickle and pulse flow (eqs 5 and 9[b])	89	26	30	150	476
pulse flow (eq 19[b])	70	15	13	>300	>300
pulse flow (eq 28[b])	70	19	12	>300	>300
Satterfield et al.[85]					
trickle flow	489	45	32	100	308
pulse flow	203	49	31	157	>300
Lemay et al.[81,c]	57	74.8	104.6	>500	>500
Burghardt and Bartelmus[148,c]				>500	>500
Boelhouwer[70]	75	5	5.4	109	315
Lakota and Levec[78]	75	15	20	22[d]	28
ANN, training file	630			15	15
ANN, test file	269			16	12
ANN, correlation	899			15.4	14
Packed Bubble Column					
Coppola et al.[155]				64.3	21.9
Goto et al.[17,e]				50.7	24.3
Jadhav and Pangarkar[150]				63	37.9
Kikuchi et al.[149,f]				78.8	78.1
Kirillov and Nasamanyan[114]				82.3	68.9
Mochizuki[156]				61.3	50.6
Specchia et al.[87]	144	33.3	39.0	88	133
Yoshikawa et al.[89,a]	49	49.3	36.7	53	52

[a] Applicable for $0.2 < Re_l < 50$ (91 data). [b] Equation's number in the original work. [c] Valid for fully wetted particles. [d] Necessitates knowledge of dynamic liquid holdup (92 data). [e] Applicable for $Re_l < 20$ (87 data). [f] Valid for $570 < Sc_l < 1420$ (115 data).

These correlations can be used for partially wetted ($\eta_e < 1$) or totally wetted ($\eta_e = 1$) beds, except those from refs 81 and 148, which are valid under full wetting conditions. A comparison between these two approaches can be found in Rode et al.[95] From Table 15 it can be concluded that $\eta_e k_{ls}$ predictions by these correlations are generally good as long as estimations are being carried out within the correlations' valid range. Venturing outside the database valid range can be disastrous. Comparatively, the present neural network correlation is almost 4 times better than the best literature correlation.[78] Figure 3 depicts parity plots of the predicted versus experimental liquid-particle mass-transfer coefficients on the training and test data sets. The data fall within the interval limits of ± 2 AARE $= \pm 30\%$.

(b) Packed Bubble Column. As shown in Table 15, the $\eta_e k_{ls}$ correlations for packed bubble columns generally perform better than those corresponding to trickle beds. This is likely ascribable to the narrow breadth of the database due to less coverage by literature studies in the case of packed bubble columns (only 230 $\eta_e k_{ls}$ data versus 899 $\eta_e k_{ls}$ data for trickle beds). All of the correlations related $\eta_e Sh_{ls}$ to the interstitial/superficial fluid Reynolds numbers except that of Kikuchi et al.,[149] who expressed the liquid-particle mass-transfer coefficient in terms of an energy dissipation. The recommended literature correlations are those of Goto et al.[17]

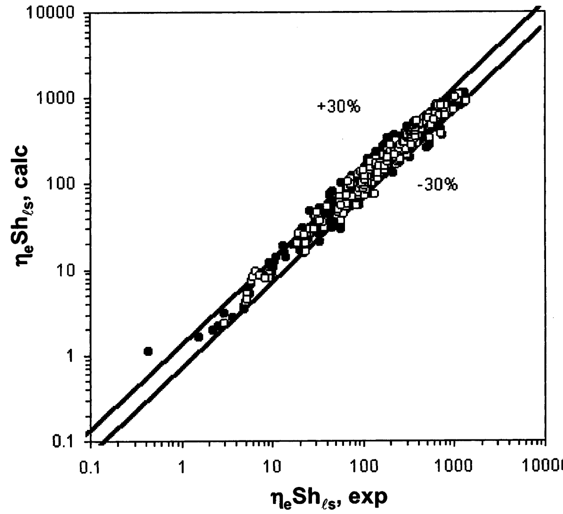

Figure 3. Correlation predictions versus experimental liquid−solid mass-transfer coefficients in trickle beds in terms of $\eta_e Sh_{ls}$ number: (●) training data set; (○) test data set.

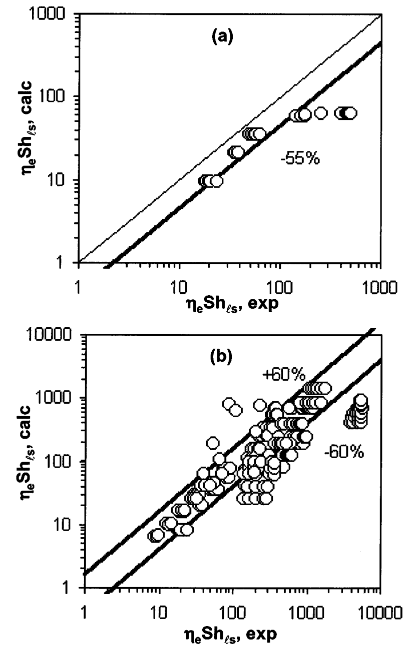

Figure 4. Correlation predictions of the liquid−solid mass-transfer coefficient in packed bubble columns in terms of the $\eta_e Sh_{ls}$ number: (a) Goto et al.;[17] (b) Jadhav and Pangarkar.[150]

for $Re_l < 20$ and Jadhav and Pangarkar[150] over the whole database; see parity plots in Figure 4a,b, respectively. Because of the scarcity of $\eta_e k_{ls}$ data in this flow configuration, we do not attempt the development of a new correlation.

Liquid-to-Wall Mass-Transfer Coefficient. (a) Trickle Bed. Here also the rareness of $\eta_e k_{lw}$ data in trickle beds (only 234 data) dissuades proposition of a new correlation. Instead, the three correlations available in the literature to predict $\eta_e k_{lw}$ are examined. Their performance against the data collected in the database is provided in Table 16. The first two correlations[72,92] relate $\eta_e k_{lw}$ to a Reynolds number (both interstitial and superficial velocity based), whereas the third correlation[93] expresses the mass-transfer coefficient as a function of the Kolmogorov group. According to Table 16 statistical results, the trickle-flow regime correlation of Latifi et al.[92] and the pulse-flow and bubble-flow regime

Table 16. Performance of Literature Correlations for the Wall Mass-Transfer Coefficient $\eta_e k_{lw}$

correlation	statistical parameter: no. of data	AARE (%)	σ (%)
Trickle Bed			
Gabitto and Lemcoff[90]	125[a]	56.8	19.6
Latifi et al.[92]			
trickle flow (eq 7[b])	117	14.7	17.3
pulse flow (eq 8[b])	75	27.9	42.5
bubble flow (eq 9[b])	29	86.3	17.2
Latifi et al.[93]			
pulse flow	75	18.4	34.6
bubble flow	29	23.5	12.2
Packed Bubble Column			
Yasunishi et al.[117]	23	31.5	10.0

[a] Pulse-flow regime. [b] Equation's number in the original work.

Table 17. Performance of Literature and Present Correlations To Predict the Wall Heat-Transfer Coefficient

ref	author's correlation within the database valid range: no. of data	AARE (%)	σ (%)	author's correlation over the whole database: AARE (%)	σ (%)
Trickle Bed					
Wild et al.[143]	125	29	13	43	40
Purwasasmita[33]	254	21	18	48	92
Muroyama et al.[129]	64	34	28	47	45
Specchia and Baldi[120,a,b]	53	64	13	74	91
ANN, training file	355			14.0	16.7
ANN, test file	153			13.4	12.7
ANN, correlation	507			14.0	15.6
Packed Bubble Column					
Sokolov and Yablokova[151]	423			64	28

[a] For the low interaction flow regime (130 data). [b] In the high interaction regime, $h_w = 2100$ W/m^2·K.

correlations of Latifi et al.[93] can be recommended for the estimation of the liquid-to-wall mass-transfer coefficient.

(b) Packed Bubble Column. The only work on the liquid−solid mass-transfer coefficient at the reactor wall in packed bubble columns reported in the literature is that of Yasunishi et al.,[117] who studied the effects of gas and liquid flow rates on $\eta_e k_{lw}$. The correlation expresses $\eta_e k_{lw}$ as a function of energy dissipation across the bed. The statistics of this correlation on the authors' own data is given in Table 16.

Performance of Heat-Transfer Correlations

Wall Heat-Transfer Coefficient. (a) Trickle Bed. Several correlations are proposed to estimate the wall heat-transfer coefficient in trickle beds. The best one, as shown in Table 17, is that of Wild et al.[143] where the Nüsselt group is expressed as a function of the liquid Reynolds and Prandtl numbers and the liquid holdup. The correlation proposed in this work is valid for all of the flow regimes and improves the predictions by almost a factor of 3; see the parity plot in Figure 5a.

(b) Packed Bubble Column. The only correlation available in the literature to estimate the wall heat-transfer coefficient in upflow is that of Sokolov and Yablokova.[151] Its performance over the database is given in Table 17. In this correlation, the Nüsselt number is correlated as a function of the liquid Prandtl and

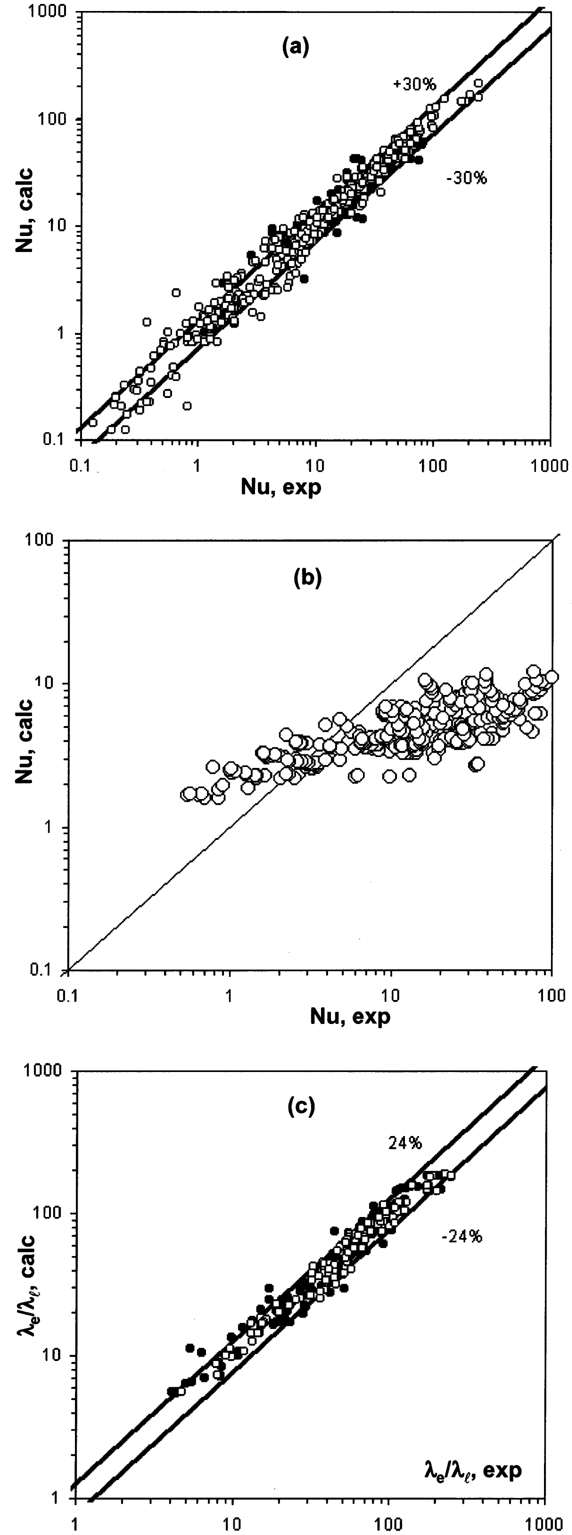

Figure 5. Correlation predictions of (a) wall heat-transfer coefficient in terms of Nu number in trickle beds, (b) in packed bubble columns using the Sokolov and Yablokova[151] correlation, and (c) effective radial thermal conductivity in trickle beds: (●) training data set; (○) test data set.

interstitial Reynolds numbers. According to Figure 5b, the liquid holdup alone that intervenes via the liquid interstitial velocity in the Re group is not sufficient to account for the influence of gas flow conditions on h_w in packed bubble columns.

Effective Radial Thermal Conductivity. (a) Trickle Bed. Among the correlations proposed in the

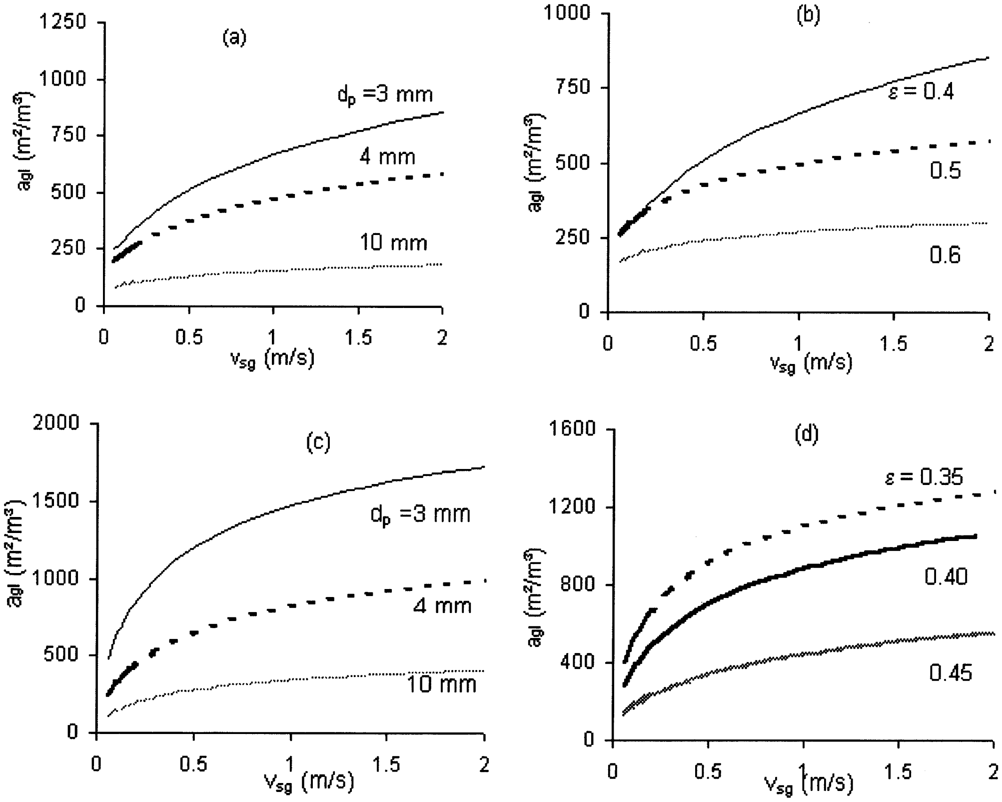

Figure 6. Effect of the bed properties on a_{gl}. Air−sulfite solution−glass beads (v_{sl} = 2 cm/s, $\rho_{l(g)}$ = 1000 (1.2) kg /m^3, $\mu_{l(g)}$ = 1.9 (1.8 × 10^{-2}) mPa·s, σ_l = 72 mN/m, d_c = 0.1 m). Trickle beds: (a) particle size (ϵ = 0.4); (b) bed porosity (d_p = 3 mm). Packed bubble column: (c) particle size (ϵ = 0.4); (d) bed porosity (d_p = 2.4 mm).

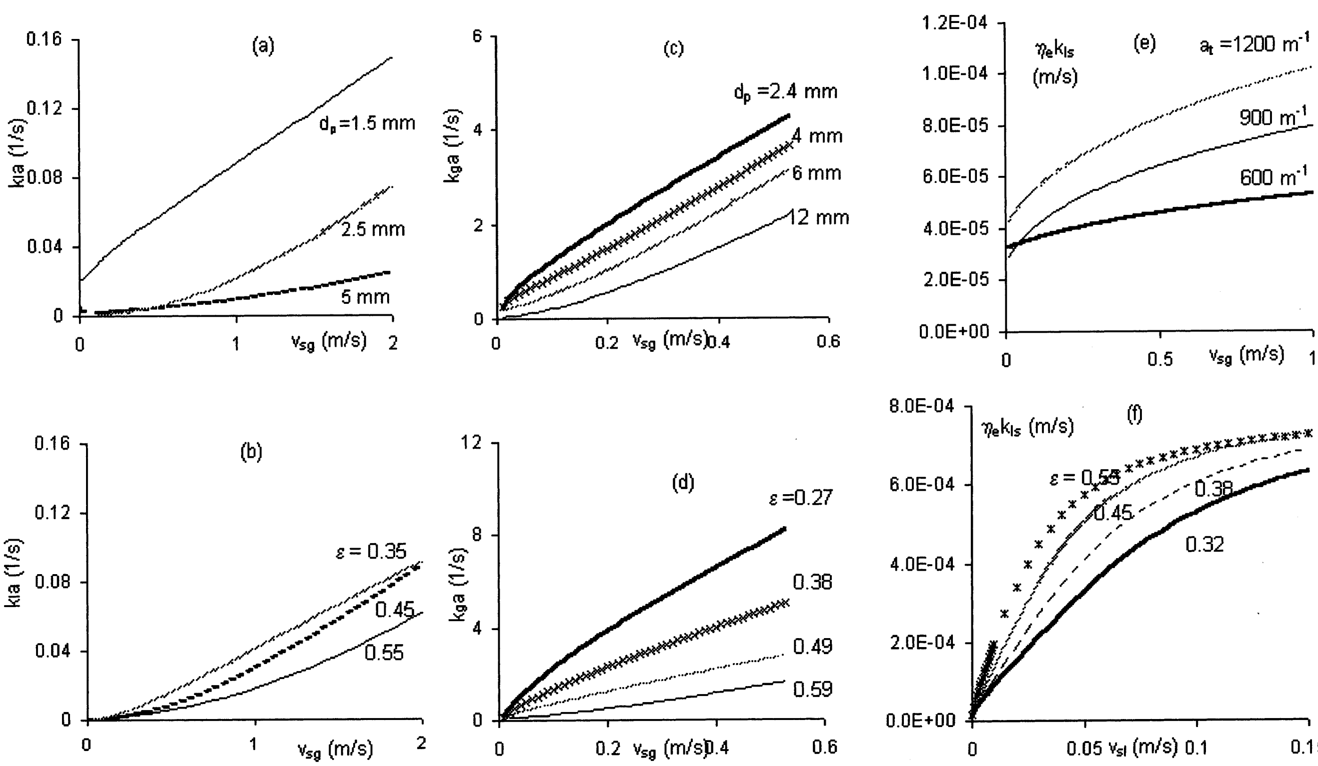

Figure 7. Effect of the bed properties on k_la: air + CO_2−ethanol + DEA solution−glass beads ($\rho_{l(g)}$ = 819 (1.7) kg/m^3, $\mu_{l(g)}$ = 1.9 (1.8 × 10^{-2}) mPa·s, σ_l = 24 mN/m, d_c = 0.05 m, H = 0.5 m); (a) particle size (ϵ = 0.4, v_{sl} = 4.4 mm/s); (b) bed porosity (d_p = 5 mm, v_{sl} = 4.4 mm/s). Effect of the bed properties on k_ga: air + CO_2−NaOH solution−glass beads (v_{sl} = 5 mm/s, $\rho_{l(g)}$ = 1000 (1.2) kg/m^3, $\mu_{l(g)}$ = 1 (1.8 × 10^{-2}) mPa·s, d_c = 0.05 m); (c) particle size (ϵ = 0.42); (d) bed porosity (d_p = 2.4 mm). Effect of the bed properties on $\eta_e k_{ls}$: air−water−benzoic acid spheres ($\rho_{l(g)}$ = 1000 (1.2) kg/m^3, $\mu_{l(g)}$ = 1 (1.8 × 10^{-2}) mPa·s, d_c = 0.1 m); (e) particle size (ϵ = 0.4, v_{sl} = 2 cm/s); (f) bed porosity (d_p = 1.5 mm, v_{sg} = 2 cm/s).

literature to predict λ_e, one can cite that of Chu and Ng[152] based on the effective medium theory and random walk analysis and that of Crine[118] based on the liquid flow maldistribution and effective particles' wettability.

Table 18. Performance of Literature and Present Correlations To Predict the Effective Radial Thermal Conductivity

ref	author's correlation within the database valid range			author's correlation over the whole database	
	no. of data	AARE (%)	σ (%)	AARE (%)	σ (%)
Trickle Bed					
Crine[118,a]				44	29
Chu and Ng[152,a]				44	53
Hashimoto et al.[122,123]	34	19	14	91	154
Specchia and Baldi[120]	35	15	17	62	96
ANN, training file	264			12.7	12.2
ANN, test file	112			11.7	8.5
ANN, correlation	376			12.4	11.3
Packed Bubble Column					
Colli-Serano and Midoux[137,b]	135	>300	>300	>500	>500
Gutsche[133,c]				24.8	22
Lamine et al.[135,b]	135	26.5	23.7	32.5	34
Sokolov and Yablokova[151,b]	135	53	27.5	69.7	86
Nakamura et al.[125,c,d]	90	90	117	>500	>500

[a] Applicable for trickle flow. [b] Valid for bubble flow. [c] Applicable for Re_g < 10 (separated flow) (120 data). [d] Valid for pulse flow.

These two approaches are valid for the trickle-flow regime, where they yield acceptable performances as shown in Table 18. The correlations of Specchia and Baldi[120] and of Hashimoto et al.[122,123] proposed for both the low and high interaction regimes take into account the liquid-phase evaporation by means of the specific heat capacity of the saturated gas. This specific heat needs to be determined from the overall heat balance using an iterative procedure. The prediction of the experimental effective radial thermal conductivity using these correlations is not very good, as shown from the statistics of Table 18. On the contrary, the correlation proposed in this work, which is valid for both the low and high interaction regimes, yields an average absolute relative error of 12%; see also the parity plot in Figure 5c.

(b) Packed Bubble Column. The few correlations proposed in the literature to predict λ_e in packed bubble columns are valid for specific flow regimes: Sokolov and Yablokova,[151] Colli-Serano and Midoux,[137] and Lamine et al.[135] for the bubble-flow regime, Nakamura et al.[125] for pulse flow, and Gutsche[133] for the separated flow regime. We recommend the use of the latter for low gas and liquid flow rates and the correlation of Lamine et al.[135] for the bubble-flow regime; see Table 18.

Particle-to-Fluid Heat-Transfer Coefficient. Studies on the heat-transfer coefficients at the particle level are very recent; only two works are reported in the literature.[131,132] In only one of them, an empirical correlation has been proposed[130] where the Nüsselt number, $h_p d_p/\lambda_L$ is expressed as a function of the Froude number, v_{sl}^2/gd_p. The performance of this correlation over the 379 experimental data (exclusively air–water–glass beads system) gives an AARE = 108% and σ = 60%.

Simulation of the Parametric Effects Using the Newly Developed Correlations

Using the neural network correlations, the effects of some fluids and bed properties on the mass- and heat-transfer characteristics are simulated.

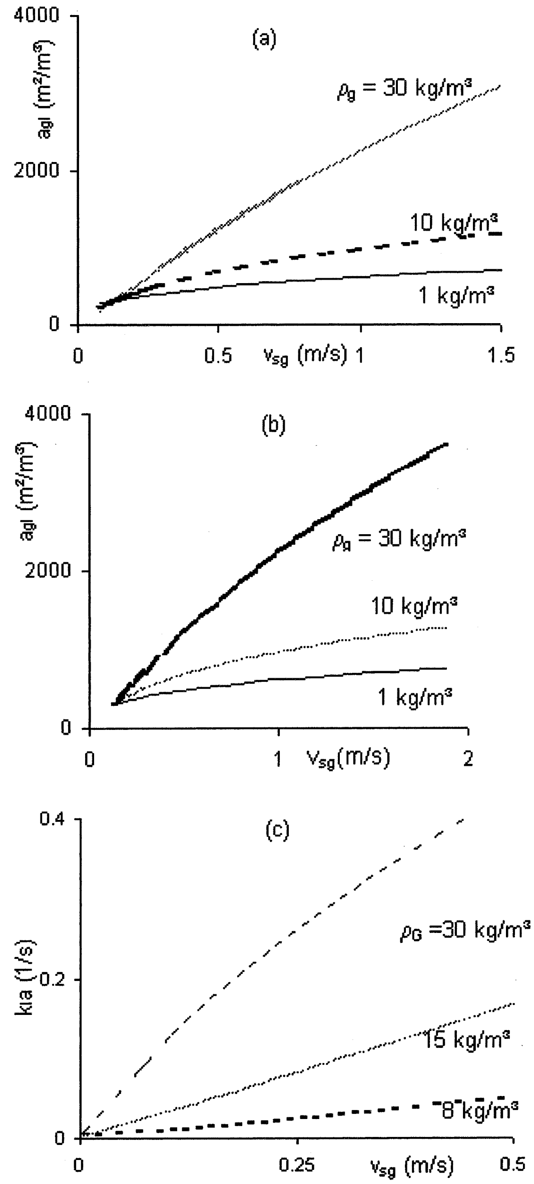

Figure 8. Effect of the gas density on a_{gl}: air–sulfite solution–glass beads (v_{sl} = 2 cm/s, $\rho_{l(g)}$ = 1000 (1.2) kg/m^3, μ_l = 1.9 mPa·s, σ_l = 72 mN/m, d_c = 0.1 m, d_p = 1.5 mm, ϵ = 0.4); (a) trickle bed; (b) packed bubble column. Effect of the gas density on $k_l a$: (c) trickle beds, air + CO_2–ethanol + DEA solution–alumina catalyst cylinders (v_{sl} = 3 mm/s, ρ_l = 819 kg/m^3, $\mu_{l(g)}$ = 1.9 (1.8 × 10^{-2}) mPa·s, σ_l = 24 mN/m, d_c = 0.05 m, H = 0.5 m, d_p = 1.77 mm, ϕ = 0.82).

(1) Mass Transfer. (a) Effect of the Particle Size and Bed Porosity. (i) On a_{gl}. In agreement with the literature results,[26,61,97,101] the gas–liquid interfacial area decreases with increasing particle size and bed porosity in trickle beds (Figure 6a,b) as well as in packed bubble columns (Figure 6c,d). Such dependencies are to be mirrored with the corresponding dependencies exhibited by the pressure drop because higher pressure drops also occasion greater interfacial areas. Furthermore, a_{gl} in upflow is greater than that in downflow, with everything else being kept identical.[100]

(ii) On $k_l a$ and $k_g a$. The influence of particle size and bed porosity on $k_l a$ in trickle-bed reactors is illustrated in Figure 7a,b, respectively. The gas–liquid interfacial area is viewed as the dominant factor undergoing reduction with an increase in the particle size and bed porosity. Hence, in agreement with the reported

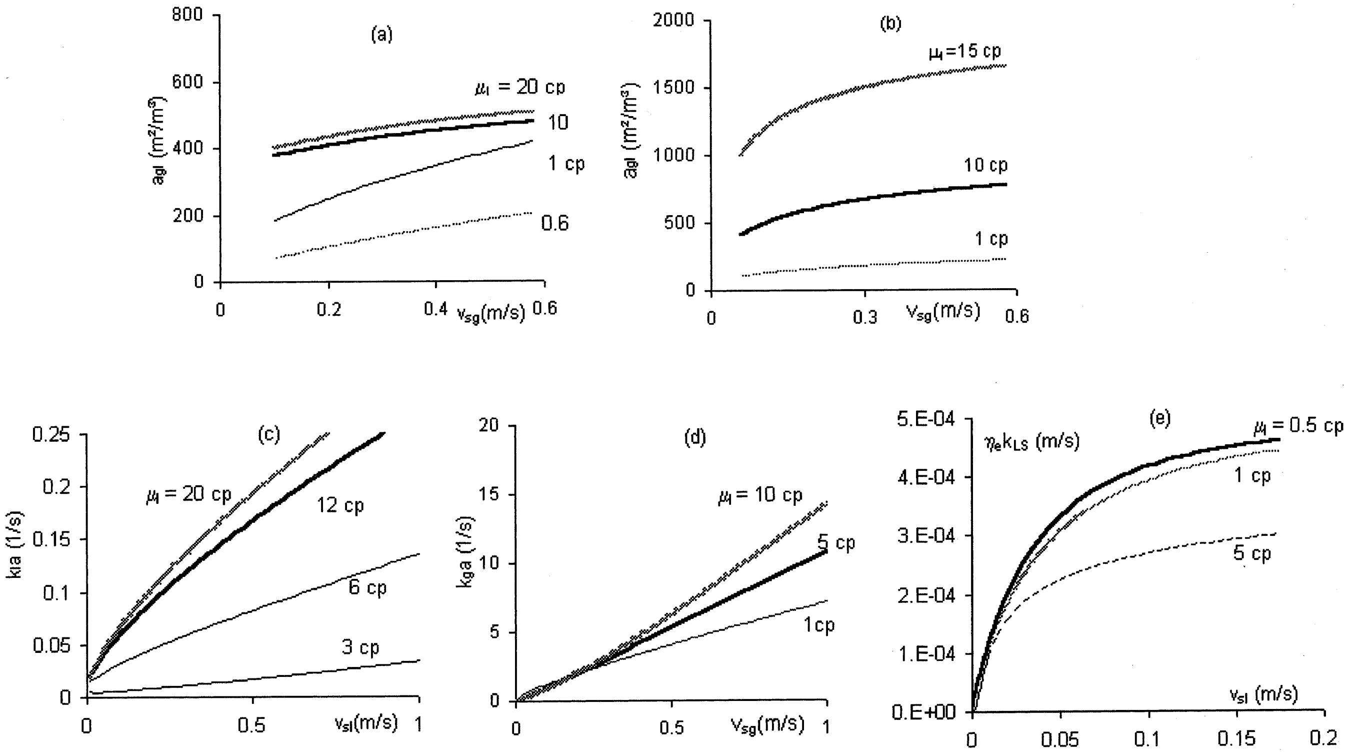

Figure 9. Effect of the liquid viscosity on a_{gl}: air−ETG−DEA solution−glass beads (v_{sl} = 2 mm/s, $\rho_{l(g)}$ = 1030 (1.2) kg/m^3, $\mu_g = 1.8 \times 10^{-2}$ mPa·s, σ_l = 71 mN/m, d_c = 0.1 m, ϵ = 0.4); (a) trickle beds (d_p = 1.5 mm); (b) packed bubble columns (d_p = 3 mm). Effect of the liquid viscosity on $k_l a$: (c) trickle beds, air + CO_2−ETG + DEA solution−alumina catalyst cylinders (v_{sg} = 4 mm/s, $\rho_{l(g)}$ = 1080 (1.7) kg/m^3, $\mu_g = 1.8 \times 10^{-2}$ mPa·s, σ_l = 48 mN/m, d_c = 0.05 m, H = 0.5 m, d_p = 1.8 mm, ϕ = 0.82). Effect of the liquid viscosity on $k_G a$: (d) trickle beds, air + CO_2−CMC + NaOH solution−glass beads (v_{sl} = 5 mm/s, $\rho_{l(g)}$ = 1000 (1.2) kg/m^3, $\mu_g = 1.8 \times 10^{-2}$ mPa·s, d_c = 0.05 m). Effect of the liquid viscosity on $\eta_e k_{ls}$: (e) trickle beds, air−CMC + potassium ferro/ferricyanide solution−glass beads (v_{sg} = 20 cm/s, $\rho_{l(g)}$ = 1000−1021 (1.2) kg/m^3, $\mu_g = 1.8 \times 10^{-2}$ mPa·s, d_c = 0.05 m, d_p = 1.4 mm, ϵ = 0.4).

observations,[12,19] $k_l a$ decreases when both such bed properties increase. Similar behavior holds true for $k_g a$ (Figure 7c,d) in agreement with literature observations.[17,43−45]

(iii) On $\eta_e k_{ls}$. The influence of particle size on $\eta_e k_{ls}$ is not clear, and the literature has not yet reached a consensus. While some authors[77,85,88] report that $\eta_e k_{ls}$ gets smaller the larger the particle size, others[83,87,153] observe exactly the opposite trend. In addition, Goto et al.,[17] using 0.54, 1.1, and 2.4 cm diameter β-naphthol and naphthalene particles, observe no effect of particle size on $\eta_e k_{ls}$. Such discrepancies cannot be ascribed to different measuring techniques being used. As a matter of fact, different authors adopting the very same measuring technique reach opposite conclusions, e.g., the dissolution technique used in refs 7, 17, 77, 85, and 87. Moreover, the flow regimes cannot be incriminated in such discrepancies because several studies being carried out in the same flow regime attain conflicting conclusions.[83,85] It seems that $\eta_e k_{ls}$ exhibits a complex nonmonotonic behavior with respect to the operating conditions explored by different investigators.

The effect of the flow configuration, i.e., upflow versus downflow, is also not unanimous. Specchia et al.[87] and Goto et al.[17] compared solid-particle mass-transfer coefficients in up- and downflow and reported higher values for upflow, which they attributed to the higher energy dissipation in the bed. On the other hand, in the range explored by Yoshikawa et al.,[89] $\eta_e k_{ls}$ is nearly insensitive to the flow configuration.

The simulations carried out using the new correlation displayed in Table 8 show that the liquid−solid mass-transfer coefficient in trickle beds decreases with increasing particle size (or equivalently decreasing external packing area, a_t) for the range of liquid and gas flow rates selected in Figure 7e, whereas it is an increasing function of bed porosity as depicted in Figure 7f. This latter effect may be explained by the fact that $\eta_e k_{ls}$ increases because of increasing interstitial liquid velocity (or decreasing liquid holdup for higher porosity) as reported, for example, by Rao and Drinkenburg.[83]

(b) Effect of the Gas Density. (i) On a_{gl}. Figure 8a illustrates the influence of the gas density on the gas−liquid interfacial area in trickle-bed reactors. Coherent with the *correlative* increase in pressure drop,[25,26] a_{gl} increases with the gas density above a critical value of gas velocity as observed by Larachi et al.[24,26,49,50] and Wammes et al.[65,66] The same effect is also typical of the upflow mode (Figure 8b).

(ii) On $k_l a$ and $k_g a$. The positive effect of the gas density (or pressure) on $k_l a$, shown in Figure 8c, is very likely due to the enhancement of a_{gl}, although the effect on k_l of the gas density is not clearly established.[24] Simulations of the pressure effect on $k_g a$ are not performed because the validity range of the present correlation is restricted to $1.12 \le \rho_g \le 1.6$ kg/m^3 (see Table 1). In fact, not a single study documents in the open literature the impact of the gas density on the gas-side volumetric mass-transfer coefficients in trickle beds and packed bubble columns.

(iii) On $\eta_e k_{ls}$. This effect is not included in the correlation proposed in Table 8 because the role of the gas density is not clearly demonstrated in the literature. Correlations where the gas density is accounted for[71,77,83,128] are not reliable except in their range of applicability (Table 15). Some authors consider the effect

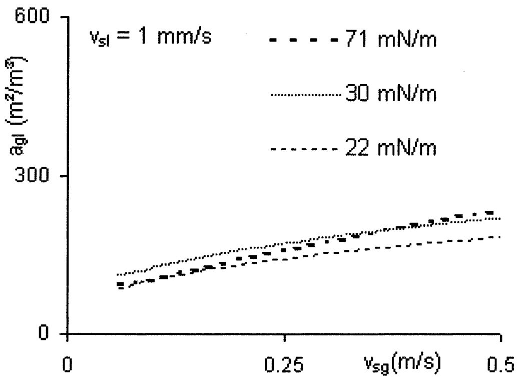

Figure 10. Effect of the surface tension on a_{gl}: air−sulfite solution−glass beads in a trickle bed (v_{sl} = 2 cm/s, $\rho_{l(g)}$ = 1000 (1.2) kg/m^3, $\mu_{l(g)}$ = 1 (1.8 × 10^{-2}) mPa·s, d_c = 0.1 m, d_p = 1.5 mm, ϵ = 0.4).

of the gas density indirectly through the pressure drop via the Kolmogorov group, which is not always accurately estimated.

On the other hand, a study by Satterfield et al.[85] where the gas density was varied using helium, nitrogen, and argon showed that gas-relevant variables such as velocity and mass flux (or equivalently Reynolds number) are inefficient to correlate $\eta_e k_{ls}$. Recently, Highfill and Al-Dahhan[76] carried out a specific study on the influence of pressure at high gas velocity. At high gas velocity, increased pressures yield higher liquid−solid mass-transfer coefficients, although it is still not clearly established at which pressure threshold this effect becomes noticeable. More work covering wider ranges of the reactor pressure, fluid flow rate, and different bed characteristics are still necessary to draw clear-cut conclusions on the effects of the gas phase.

(c) Effect of the Liquid Viscosity. (i) On a_{gl}. The influence of the liquid viscosity is shown in Figure 9a,b, respectively, for trickle beds and packed bubble columns. An increase in the liquid viscosity induces an increase in the gas−liquid interfacial area in a manner similar to that for pressure drop and liquid holdup.[11,24,25,29,30,50,54,97]

(ii) On k_la and k_ga. Similar effect is observed for k_la (Figure 9c) in trickle beds. The increase in k_la as a function of an increase in the liquid viscosity is imputed likely to the increased gas−liquid interfacial area as shown above and also as interpreted by several authors.[21,24,28,29]

The liquid viscosity affects the gas-side mass-transfer coefficient only above a critical value of the gas velocity (Figure 9d). The influence of the liquid viscosity on k_ga has not been specifically studied in the literature. However, Yaïci reported,[43] using different reacting systems in trickle beds (aqueous, organic, foaming, and nonfoaming), that higher k_ga values are yielded by the more viscous liquids.

(iii) On $\eta_e k_{ls}$. The only known work reporting the effect of the liquid viscosity on $\eta_e k_{ls}$ is that of Gabitto and Lemcoff[72] where CMC solutions have been used in trickle beds. The simulated results using the correlation

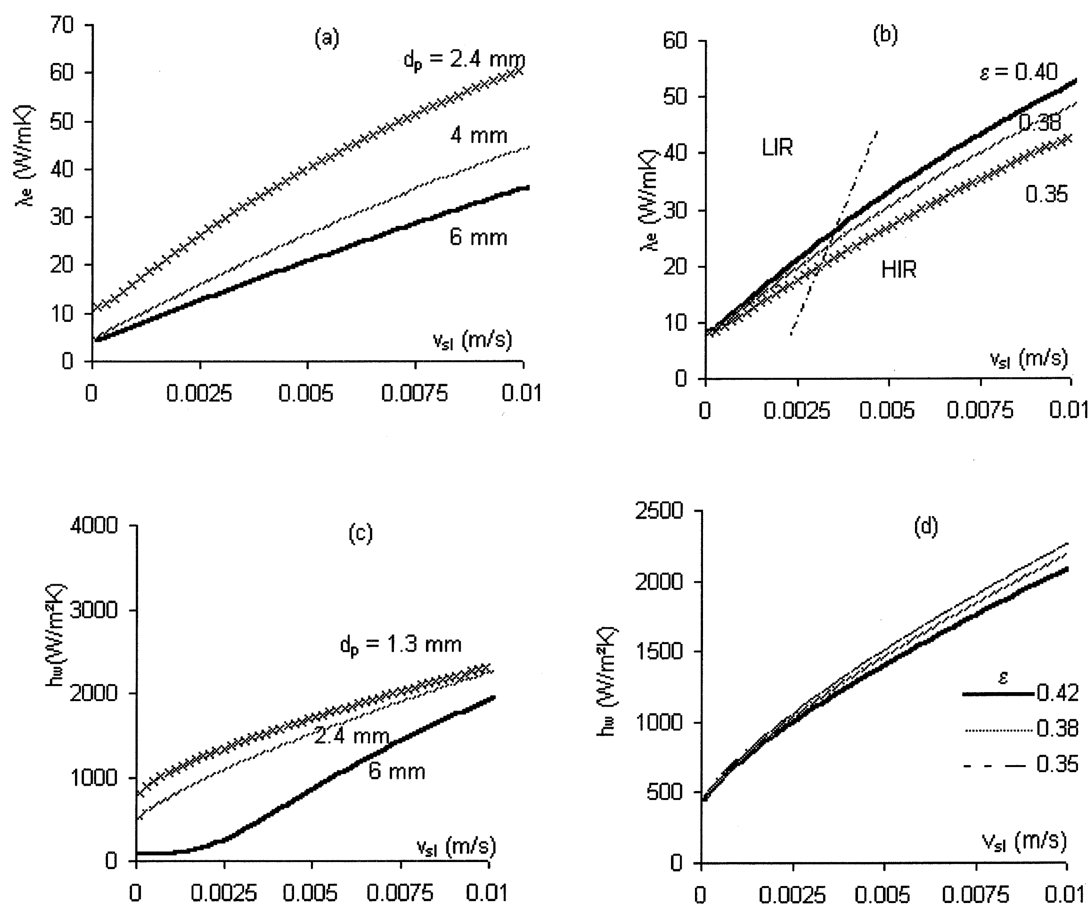

Figure 11. Effect of the bed properties on λ_e in trickle beds: air−water−glass beads (v_{sg} = 2 cm/s, $\rho_{l(g)}$ = 1000 (1.2) kg/m^3, $\mu_{l(g)}$ = 1 (1.8 × 10^{-2}) mPa·s, σ_l = 72 mN/m, d_c = 0.1 m); (a) particle size (ϵ = 0.42); (b) bed porosity (d_p = 2.4 mm). Effect of the bed properties on h_w in trickle beds: air−water−glass beads (v_{sg} = 2 cm/s, $\rho_{l(g)}$ = 1000 (1.2) kg/m^3, $\mu_{l(g)}$ = 1 (1.8 × 10^{-2}) mPa·s, σ_l = 72 mN/m, d_c = 0.1 m); (c) particle size (ϵ = 0.42); (d) bed porosity (d_p = 2.4 mm).

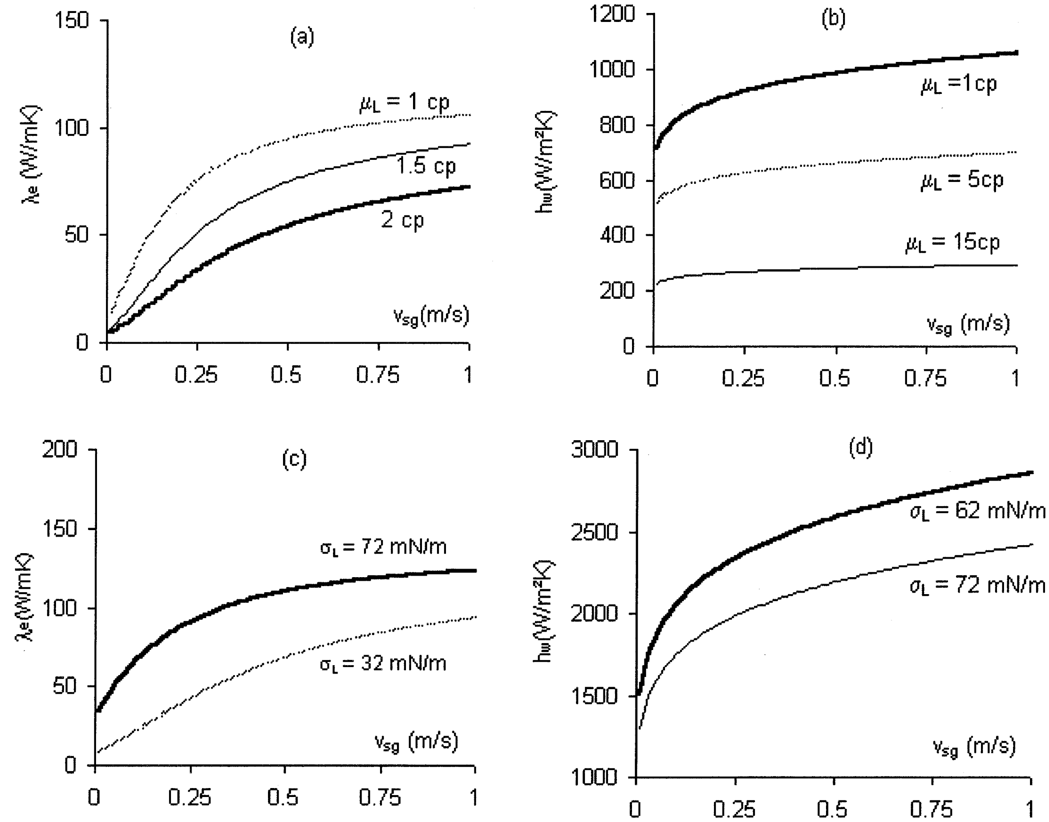

Figure 12. Effect of the liquid viscosity on (a) λ_e and (b) h_w in trickle beds: air−CMC solutions−glass beads (v_{sg} = 2 cm/s, $\rho_{l(g)}$ = 1000−1010 (1.2) kg/m^3, $\mu_g = 1.8 \times 10^{-2}$ mPa·s, σ_l = 72 mN/m, d_c = 0.1 m, ϵ = 0.42, d_p = 2.4 mm). Effect of the surface tension on (c) λ_e and (d) h_w in trickle beds: air−water + surfactant−glass beads (v_{sl} = 5 mm/s, $\rho_{l(g)}$ = 1000 (1.2) kg/m^3, $\mu_{l(g)} = 1\ (1.8 \times 10^{-2})$ mPa·s, d_c = 0.1 m, ϵ = 0.42, d_p = 2.4 mm).

from Table 8 show a negative effect of the liquid viscosity on $\eta_e k_{ls}$ in trickle beds (Figure 9e), coherent with the study of Gabitto and Lemcoff.[72] However, more experimental work is still needed to establish whether this trend is general and especially for packed bubble columns, for which not a single study is available to answer this question.

(d) Liquid Foaming Ability and Surface Tension. (i) On a_{gl}, $k_l a$, and $k_g a$. Several authors report that liquid foaminess or liquid coalescence inhibition induces drastic enhancement in the gas−liquid interfacial area in trickle beds[11,28,29,33,54,65,66] as well as in packed bubble columns.[97] On the other hand, the influence of liquid surface tension is not observed,[28,29,54] and the simulations shown in Figure 10 for trickle beds support this conclusion. A similar simulation pattern is observed for the upflow mode.

Subtended by the effect on the gas−liquid interfacial areas, $k_l a$ values are more important when foaming liquids are used.[29,33] However, the influence of surface tension has not been specifically addressed over the concerned literature. The simulations using the presently developed correlation for trickle beds yield no effect of surface tension on $k_l a$ (figure not shown). Regarding the liquid surface tension and foaminess, their effects on $k_g a$ remain marginal, as observed in the literature.[11,43,45] Consequently, both effects are also disregarded in the developed correlation shown in Table 6.

(ii) On $\eta_e k_{ls}$. Referring to the works summarized in Table 15, the influence of the liquid surface tension has been mostly ignored with the exception of one work.[87] However, despite these latter authors incorporating this variable as a correlating variable via a liquid Weber number, they reported a persistent scatter in their correlated data. Therefore, surface tension is not considered in the correlation proposed in this work; see Table 8.

(2) Heat Transfer. (a) Effect of the Particle Size and Bed Porosity. In Figure 11a is depicted the particle size effect on the effective radial thermal conductivity, λ_e, in trickle-bed reactors. As reported by Specchia and Baldi,[120] the effective radial thermal conductivity in the bed decreases with increasing particle size plausibly because of the reduction of liquid holdup. Bed porosity changes, as shown in Figure 11b, act only marginally on λ_e in the trickle-flow regime. However, λ_e undergoes a slight enhancement when the liquid velocity increases, giving rise to higher liquid holdups in the high interaction flow regime.

The effect of the particle size on the wall heat-transfer coefficient, h_w, is illustrated in Figure 11c. It appears that the wall heat-transfer coefficient increases with a decrease in the particle diameter, with a tendency of leveling off toward the smaller particle diameters. Bed porosity has virtually no influence, as suggested by Figure 11d simulations, over the range of porosity from 0.35 to 0.42. From the works reported in the literature,[33,120] no remarkable effect of the bed porosity on h_w has been observed. Regarding the column-to-particle diameter ratio, the Mariani et al.[161] experimental results pointed to an apparent limitation of the two-dimensional pseudohomogeneous plug-flow models usually used to model heat-transfer parameters in fixed beds. According to their findings, the recommended ratio should be larger than 15 to keep the model valid.

(b) Effect of the Liquid Viscosity. The liquid viscosity effect on λ_e and h_w, shown respectively in parts a and b of Figure 12, suggests that higher viscosity liquids deteriorate the heat-transfer ability in trickle beds. Two reasons could be causing such poor heat transfer for higher viscosity liquids: (i) the lower thermal conductivity and specific heat capacity; (ii) the lower degree of lateral mixing. This is corroborated by the experimental observations reported in the literature using water and different ethylene glycol solutions[33,119,124] and CMC solutions.[154]

(c) Effect of the Surface Tension. The influence of the surface tension is antagonistic regarding λ_e and h_w. Lower σ_l gives lower λ_e (Figure 12c) but higher h_w (Figure 12d). These simulations correspond to the low interaction flow regime. A decrease in the radial effective heat-transfer coefficient when low surface tension liquids are used could be explained by the presence of higher gas holdup, which induces poorer radial heat transfer. However, this interpretation cannot explain why the wall heat-transfer increases. It is worth mentioning that Lamine et al.[135] observed exactly the opposite effects for the packed bubble columns in the bubble-flow regime. No explanation was given for their observations.

Conclusion

The following correlations are recommended for estimation: (i) the ANN correlation in Table 5 for k_la in trickle-bed reactors; (ii) the k_la correlation of Saada[98] for packed bubble columns; (iii) the ANN correlation in Table 6 for k_ga in trickle-bed reactors; (iv) neither k_ga measurements nor a correlation for packed bubble columns; (v) the ANN correlation in Table 7 for a in trickle-bed reactors; (vi) the ANN correlation in Table 11 for a in packed bubble columns; (vii) the ANN correlation in Table 8 for $\eta_e k_{ls}$ in trickle-bed reactors; (viii) the $\eta_e k_{ls}$ correlations of Goto et al.[17] (for $Re_l < 20$) and of Jadhav and Pangarkar[150] for packed bubble columns; (ix) the $\eta_e k_{lw}$ liquid-to-wall mass-transfer coefficient correlations of Latifi et al.[92,93] for trickle-bed reactors; (x) the $\eta_e k_{lw}$ liquid-to-wall mass-transfer coefficient correlation of Yasunishi et al.[117] for packed bubble columns; (xi) the ANN correlation in Table 9 for h_w for trickle-bed reactors; (xii) the h_w wall heat-transfer coefficient correlation of Sokolov and Yablokova[151] for packed bubble columns; (xiii) the ANN correlation in Table 10 for λ_e for trickle-bed reactors; (xiv) the λ_e effective radial thermal conductivity correlations of Gutsche[133] in the separated-flow regime and of Lamine et al.[135] for the bubble-flow regime in packed bubble columns; (xv) the h_p particle-to-fluid heat-transfer coefficient of Marcandelli[130] in trickle-bed reactors; (xvi) neither h_p measurements nor a correlation for packed bubble columns.

Acknowledgment

Financial support from the Natural Sciences and Engineering Research Council of Canada (NSERC) and the Fonds pour la formation de chercheurs et d'aide à la recherche is gratefully acknowledged.

Nomenclature

a_{gl} = gas−liquid interfacial area, m^2/m^3
a_t = external packing area, external surface packing per unit reactor volume, m^2/m^3
a_s = external area of particles and wall per unit reactor volume = $a_t + 4/d_c$, m^2/m^3
AARE = average absolute relative error = $(1/N)\sum_{i=1}^{N}|(y_{calc,i} - y_{exp,i})/y_{exp,i}|$
$C_{p\alpha}$ = α-phase heat capacity, J/kg·K
d_c = column diameter, m
d_h = Krischer and Kast hydraulic diameter = $d_p[16\epsilon^3/9\pi(1 - \epsilon)^2]^{1/3}$
d_h' = Krischer and Kast hydraulic diameter = $d_p'[16\epsilon^3/9\pi(1 - \epsilon)^2]^{1/3}$
d_p = equivalent particle diameter defined as the diameter of an equal-volume sphere, m
d_p' = equivalent particle diameter defined as the diameter of an equal-area sphere, m
D_α = α-phase diffusivity, m^2/s
Eo_l = liquid Eotvos number
Fr_α = α-phase Froude number
g = gravitational acceleration, m/s^2
h_p = particle-fluid heat-transfer coefficient, W/m^2·K
h_w = wall heat-transfer coefficient, W/m^2·K
H = packed bed height, m
J = number of nodes in the hidden layer
$k_\alpha a$ = α-phase side volumetric mass-transfer coefficient, s^{-1}
$\eta_e k_{ls}$ = liquid-particle mass-transfer coefficient, m/s
$\eta_e k_{lw}$ = liquid-wall mass-transfer coefficient, m/s
N = number of data
Nu = Nüsselt number
P = pressure, Pa
Pe_α = α-phase heat Péclet number
Pe_{gl} = composite heat Péclet number
Re_α = α-phase Reynolds number
S_b = bed correction function
Sc_α = α-phase Schmidt number
Sh_α = α-phase Sherwood number
St_{gl} = composite Stokes number
St_l = liquid Stokes number
T = temperature, K
$v_{s\alpha}$ = α-phase superficial velocity, m/s
We_α = α-phase Weber number

Greek Letters

ϵ = bed porosity
$\mathbf{\Gamma}$ = hidden-layer vector
ϕ = sphericity factor
η_e = wetting efficiency
λ_α = α-phase thermal conductivity, W/m·K
λ_e = effective radial thermal conductivity, W/m·K
μ_α = α-phase dynamic viscosity, Pa·s
ω = connectivity weights
ρ_α = α-phase density, kg/m^3
σ = standard deviation = $\{[1/(N - 1)]\sum_{i=1}^{N}[|(y_{calc,i} - y_{exp,i})/y_{exp,i}| - \mathrm{AARE}]^2\}^{1/2}$
σ_l = surface tension, N/m
Ω_i = network normalized input variables
Ψ = network output

Subscripts

α = gas or liquid
calc = calculated
exp = experimental
G = gas phase
L = liquid phase
s = solid phase

Abbreviations

CHA = cyclohexylamine
CMC = carboxymethylcellulose
DEA = diethanolamine

DIPA = di-2-propanolamine
DMA = dimethylamine
ETG = ethylene glycol
EtOH = ethanol
IPA = isopropropanolamine
MEA = monoethanolamine
i-PrOH = 2-propanol
PE = polyethylene
PP = polypropylene
PVC = poly(vinyl chloride)

Literature Cited

(1) Dudukovic, M. P.; Larachi, F.; Mills, P. L. Multiphase reactors—Revisited. *Chem. Eng. Sci.* **1999**, *54*, 1975.

(2) Dudukovic, M. P.; Larachi, F.; Mills, P. L. Multiphase catalytic reactors: A perspective on current knowledge and future trends. *Catal. Rev.* **2002**, *44*, 123.

(3) Chen, Y. W.; Tsai, M. C. Hydrodrodesulfurization of atmospheric gas oil over NiMo/aluminum borate catalysts in a trickle-bed reactor. *Ind. Eng. Chem. Res.* **1997**, *36*, 2521.

(4) Landau, M. V.; Herskowitz, M.; Givoni, D.; Laichter, S.; Yitzhaki, D. Medium severity hydrotreating and hydrocracking of Israeli shale oil—II. Testing of novel catalyst systems in a trickle-bed reactor. *Fuel* **1998**, *77*, 3.

(5) Westerterp, K. R.; Wammes, W. J. A. Three-phase trickle-bed reactors, in: Principles of Chemical Reaction Engineering and Plant Design. *Ullmann's Encyclopedia of Industrial Chemistry*, 5th ed.; 1992; Vol. B4, p 309.

(6) Chou, S. H.; Chen, S. C.; Tan, C. S.; Wang, W. H. Hydrogenation of dicyclopentadiene in a trickle-bed reactor. *J. Chin. Inst. Chem. Eng.* **1997**, *28*, 175.

(7) Khadilkar, M. R.; Jiang, Y.; Al-Dahhan, M.; Dudukovic, M. P.; Chou, S. K.; Ahmed, G.; Kahney, R. Investigation of a complex reaction network: Experiments in a high-pressure trickle-bed reactor. I. *AIChE J.* **1998**, *44*, 912.

(8) Cheng, S.; Chuang, K. T. Simultaneous methanol removal and destruction from wastewater in a trickle-bed reactor. *Can. J. Chem. Eng.* **1992**, *70*, 727.

(9) Pintar, A.; Bercic, G.; Levec, J. Catalytic liquid-phase oxidation of aqueous phenol solutions in a trickle-bed reactor. *Chem. Eng. Sci.* **1997**, *52*, 4143.

(10) Wübker, S.-M.; Laurenzis, A.; Werner, U.; Friedrich, C. Controlled biomass formation and kinetics of toluene degradation in a bio-scrubber and in a reactor with a periodically moved trickle bed. *Biotechnol. Bioeng.* **1997**, *55*, 686.

(11) Azzaz, M. S. Réacteurs gaz-liquide-solide à lit fixe: Réactions catalytiques, hydrodynamique et transfert de matière. Ph.D. Thesis, Institut National Polytechnique de Lorraine, Nancy, France, 1984.

(12) Blok, J. R.; Koning, C. E.; Drinkenburg, A. A. H. Gas—liquid mass transfer in fixed-bed reactors with cocurrent downflow operating in the pulsing flow regime. *AIChE J.* **1984**, *30*, 393.

(13) Frank, M. J. W. Mass and heat transfer phenomena in G—L(—S) reactors relevant for reactive distillation. Ph.D. Thesis, Twente University, Enschede, The Netherlands, 1996.

(14) Fukushima, S.; Kusaka, K. Liquid-phase volumetric and mass transfer coefficient, and boundary of hydrodynamic flow region in packed column with cocurrent downward flow. *J. Chem. Eng. Jpn.* **1977**, *10*, 468.

(15) Gianetto, A.; Specchia, V.; Baldi, G. Absorption in packed towers with concurrent downward high-velocity flows. II—Mass transfer. *AIChE J.* **1973**, *19*, 916.

(16) Goto, S.; Smith, J. M. Trickle-bed reactor performance: Holdup and mass transfer effects. *AIChE J.* **1975**, *21*, 706.

(17) Goto, S.; Levec, J.; Smith, J. M. Mass transfer in packed beds with two-phase flow. *Ind. Eng. Chem. Process Des. Dev.* **1975**, *14*, 473.

(18) Guangda, G.; Dudukovic, M. P. Mass transfer and pressure drop in trickle beds with small particles. *J. Chem. Eng. Chin. Univ.* **1993**, *7*, 29.

(19) Hirose, T.; Toda, M.; Sato, Y. Liquid-phase mass transfer in packed bed reactor with cocurrent gas—liquid downflow. *J. Chem. Eng. Jpn.* **1974**, *7*, 187.

(20) Iliuta, I. Hydrodynamics and mass transfer in multiphase fixed bed reactors. Ph.D. Thesis, Université Catholique de Louvain, Louvain, Belgium, 1996.

(21) Iliuta, I.; Thyrion, F. C. Gas—liquid mass transfer in fixed beds with two-phase cocurrent downflow: gas/Newtonian and non-Newtonian liquid systems. *Chem. Eng. Technol.* **1997**, *20*, 538.

(22) Iliuta, I.; Iliuta, M. C.; Thyrion, F. C. Gas—liquid mass transfer in trickle-bed reactors: gas-side mass transfer. *Chem. Eng. Technol.* **1997**, *20*, 589.

(23) Lakota, A. Hydrodynamics and mass transfer characteristics of trickle-bed reactors. Ph.D. Thesis, University of Ljubljana, Ljubljana, Slovenia, 1990.

(24) Larachi, F. Les réacteurs triphasiques à lit fixe à écoulement à co-courant vers le bas et vers le haut de gaz et de liquide. Étude de l'influence de la pression sur l'hydrodynamique et le transfert de matière gaz—liquide. Ph.D. Thesis, Institut National Polytechnique de Lorraine, Nancy, France, 1991.

(25) Lara-Marquez, A.; Larachi, F.; Wild, G.; Laurent, A. Mass transfer characteristics of fixed beds with cocurrent upflow and downflow. A special reference to the effect of pressure. *Chem. Eng. Sci.* **1992**, *47*, 3485.

(26) Larachi, F.; Cassanello, M.; Laurent, A. Gas—liquid interfacial mass transfer in trickle-bed reactors at elevated pressures. *Ind. Eng. Chem. Res.* **1998**, *37*, 7, 718.

(27) Mahajani, V. V.; Sharma, M. M. Effective interfacial area and liquid side mass transfer coefficient in trickle bed reactors. *Chem. Eng. Sci.* **1979**, *34*, 1425.

(28) Midoux, N.; Morsi, B. I.; Purwasasmita, M.; Laurent, A.; Charpentier, J. C. Interfacial area and liquid side mass transfer coefficient in trickle bed reactors operating organic liquids. *Chem. Eng. Sci.* **1984**, *39*, 781.

(29) Morsi, B. I. Hydrodynamique, aires interfaciales et coefficients de transfert de matière gaz—liquide dans les réacteurs catalytiques à lit fixe arrosé: Les résultats obtenus en milieu liquide aqueux académique sont-ils encore représentatifs en milieu organique industriel? Ph.D. Thesis, Institut National Polytechnique de Lorraine, Nancy, France, 1982.

(30) Morsi, B. I.; Laurent, A.; Midoux, N.; Barthole-Delanauy, G.; Storck, A.; Charpentier, J. C. Hydrodynamics and gas—liquid-olid interfacial parameters of co-current downward two-phase flow in trickle-bed reactors. *Chem. Eng. Commun.* **1984**, *25*, 267.

(31) Morsi, B. I. Mass transfer coefficients in a trickle-bed reactor with high and low viscosity organic solutions. *Chem. Eng. J.* **1989**, *41*, 41.

(32) Patil, V. K.; Sharma, M. M. Hydrodynamics and mass transfer characteristics of co-current downflow packed tube columns. *Can. J. Chem. Eng.* **1983**, *61*, 509.

(33) Purwasasmita, M. Contribution à l'étude des réacteurs gaz—liquide à lit fixe à co-courant vers le bas à fortes vitesses du gaz et du liquide. Hydrodynamique, transfert de matière et de chaleur pour des liquides aqueux et organiques. Ph.D. Thesis, Institut National Polytechnique de Lorraine, Nancy, France, 1985.

(34) Seirafi, H. A.; Smith, J. M. Mass transfer and adsorption in liquid-full and trickle beds. *AIChE J.* **1980**, *26*, 711.

(35) Sylvester, N. D.; Pitayagulsarn, P. Mass transfer for two-phase cocurrent downflow in a packed bed. *Ind. Eng. Chem. Process Des. Dev.* **1975**, *14*, 421.

(36) Turek, F.; Lange, R. Mass transfer in trickle-bed reactors at low Reynolds number. *Chem. Eng. Sci.* **1981**, *36*, 569.

(37) Ufford, R. C.; Perona, J. J. Liquid-phase mass transfer with concurrent flow through packed towers. *AIChE J.* **1973**, *19*, 1223.

(38) Wang, R.; Mao, Z.; Chen, J. Hysteresis of gas—liquid mass transfer in a trickle bed reactor. *Chin. J. Chem. Eng.* **1994**, *2*, 236.

(39) Wang, R.; Luan, M.; Mao, Z.; Chen, J. Correlation between hysteresis of gas—liquid mass transfer and liquid distribution in a trickle bed. *Chin. J. Chem. Eng.* **1997**, *5*, 135.

(40) Martin, J. M.; Combarnous, M.; Charpentier, J. C. Physical gas—liquid mass transfer for cocurrent flow through porous medium with liquid and gas flow rates corresponding to the conditions of enhanced oil recovery. *Chem. Eng. Sci.* **1980**, *35*, 2366.

(41) Shende, B. W.; Sharma, M. M. Mass transfer in packed columns: cocurrent operation. *Chem. Eng. Sci.* **1974**, *29*, 1763.

(42) Wen, C. Y.; O'Brien, W. S.; Fan, L. T. Mass transfer in packed beds operated cocurrently. *J. Chem. Eng. Data* **1963**, *8*, 42.

(43) Yaïci, W. Mise au point de nouveaux systèmes d'absorption gaz-liquide avec réaction chimique en milieux liquides aqueux et organique en vue de leur application à la détermination par méthode chimique de la conductance de transfert de matière en phase gazeuse dans un réacteur catalytique à lit fixe arrosé. Ph.D.

Thesis, Institut National Polytechnique de Lorraine, Nancy, France, 1985.

(44) Yaïci, W.; Laurent, A.; Midoux, N.; Charpentier, J. C. Détermination des coefficients de transfert de matière en phase gazeuse dans un réacteur catalytique à lit fixe arrosé en présence de phases liquides aqueuses et organiques. *Bull. Soc. Chim. Fr.* **1985**, *6*, 1032.

(45) Yaïci, W.; Laurent, A.; Midoux, N.; Charpentier, J. C. Determination of gas-side mass transfer coefficients in trickle-bed reactors in the presence of an aqueous or an organic liquid phase. *Int. Chem. Eng.* **1988**, *28*, 299.

(46) Bakos, M.; Arva, P.; Szeifert, F. Interfacial area in packed bed gas–liquid reactors with co-current downward flow. *Hung. J. Ind. Chem.* **1980**, *8*, 383.

(47) Fukushima, S.; Kusaka, K. Interfacial area and boundary of hydrodynamic flow region in packed column with cocurrent downward flow. *J. Chem. Eng. Jpn.* **1977**, *10*, 461.

(48) Gianetto, A.; Baldi, G.; Specchia, V. Absorption in packed towers with concurrent high velocity flows. I—Interfacial areas. *Quad. Ing. Chim. Ital.* **1970**, *6*, 125.

(49) Larachi, F.; Laurent, A.; Wild, G.; Midoux, N. Pressure effects on gas–liquid interfacial area in cocurrent trickle-flow reactors. *Chem. Eng. Sci.* **1992**, *47*, 2325.

(50) Larachi, F.; Cassanello, M.; Laurent, A.; Midoux, N.; Wild, G. Gas–liquid interfacial areas in three-phase fixed bed reactors. *Chem. Eng. Process.* **1997**, *36*, 497.

(51) Mahajani, V. V.; Sharma, M. M. Mass transfer in packed columns: cocurrent (downflow) operation: 1 in. and 1.5 in. metal pall rings and ceramic Intalox saddles: multi-filament gauze packings in 20 cm and 38 cm I.D. columns. *Chem. Eng. Sci.* **1980**, *35*, 941.

(52) Midoux, N.; Wild, G.; Purwasasmita, M.; Laurent, A.; Charpentier, J. C.; Martin, H. Zum Flüssigkeitsinhalt und zum Wärmeübergang in Rieselbettreaktoren bei hoher Wechselwirkung des Gases und der Flüssigkeit. *Chem. Ing. Tech.* **1986**, *MS 1445*, 142.

(53) Mitchell, M. G.; Perona, J. J. Gas–liquid interfacial areas for high porosity tower packings in concurrent downward flow. *Ind. Eng. Chem. Process Des. Dev.* **1979**, *18*, 316.

(54) Morsi, B. I.; Midoux, N.; Laurent, A.; Charpentier, J. C. Hydrodynamique et aire interfaciale des écoulements gaz–liquide à co-courant vers le bas en lit fixe. Influence de la nature du liquide. *Entropie* **1980**, *16*, 38.

(55) Morsi, B. I.; Laurent, A.; Midoux, N.; Charpentier, J. C. Interfacial area in trickle bed reactors: Comparison between ionic and organic liquids and between Raschig rings and small diameter particles. *Chem. Eng. Sci.* **1980**, *35*, 1467.

(56) Morsi, B. I.; Midoux, N.; Laurent, A.; Charpentier, J. C. Hydrodynamics and interfacial areas in downward cocurrent gas–liquid flow through fixed beds. Influence of the nature of the liquid. *Int. Chem. Eng.* **1982**, *22*, 142.

(57) Nagel, O.; Kürten, H.; Sinn, R. Stoffaustauschfläche und Energiedissipationsdichte als Auswahlkriterien für Gas/Flüssigkeits-Reaktoren. *Chem. Ing. Tech.* **1972**, *44*, 367.

(58) Patil, V. K.; Sharma, M. M. Packed tube columns: Hydrodynamics and effective interfacial area: Pall rings and multifilament wire gauge packings. *Can. J. Chem. Eng.* **1981**, *59*, 606.

(59) Shiying, G.; Yunsheng, C.; Pangsheng, L. Study of gas-phase mass transfer coefficients in trickle beds with small particles. *J. East China Inst. Chem. Technol.* **1989**, *15*, 565.

(60) Ratnam, V. G. S.; Varma, Y. B. G. Effective interfacial area in gas–liquid cocurrent downflow through packed beds. *Bioprocess Eng.* **1991**, *7*, 29.

(61) Ratnam, V. G. S.; Narasaiah, V. D.; Varma, Y. B. G. A correlation for interfacial area in cocurrent gas–liquid downflow through packed beds. *Bioprocess Eng.* **1994**, *10*, 53.

(62) Versteeg, G. F. Mass transfer and chemical reaction kinetics in acid gas treating processes. Ph.D. Thesis, Twente University, Enschede, The Netherlands, 1987.

(63) Versteeg, G. F.; van Swaaij, W. P. M. Absorption of CO_2 and H_2S in aqueous alkanolamine solutions using a fixed-bed reactor with cocurrent downflow operation in the pulsing flow regime. *Chem. Eng. Process.* **1988**, *24*, 163.

(64) Vivarié, A. Étude de l′hydrodynamique et des aires interfaciales gaz–liquide associées à des écoulements diphasés à co-courant vers le bas dans un réacteur pilote à garnissage. Comparaison avec les résultats de la littérature obtenus à l′aide de travaux avec des colonnes de laboratoire. CNAM Thesis, Conservatoire National des Arts et Métiers de Paris, Nancy, France, 1981.

(65) Wammes, W. J. A. Hydrodynamics in a cocurrent gas–liquid trickle-bed reactor at elevated pressures. Ph.D. Thesis, Twente University, Enschede, The Netherlands, 1990.

(66) Wammes, W. J. A.; Middelkamp, J.; Huisman, W. J.; de Baas, C. M.; Westerterp, K. R. Hydrodynamics in a cocurrent gas–liquid trickle bed at elevated pressures, Part 1: gas–liquid interfacial areas, Part 2: liquid holdup, pressure drop, flow regimes. *AIChE J.* **1991**, *37*, 1849.

(67) Barthole, G. Apport de l′électrochimie à l′étude des réacteurs gaz-liquide-solide à lit fixe: hydrodynamique et transfert de matière liquide-solide. Application à l′électro-synthèse. Ph.D. Thesis, Institut National Polytechnique de Lorraine, Nancy, France, 1983.

(68) Barthole-Delaunay, C.; Storck, A.; Laurent, A.; Charpentier, J. C. Détermination électrochimique du transfert de matière liquide–solide dans un réacteur gas–liquide à lit fixe arrosé fonctionnant à co-courant vers le bas. *Entropie* **1980**, *93*, 30.

(69) Barthole-Delaunay, C.; Storck, A.; Laurent, A.; Charpentier, J. C. Electrochemical determination of liquid–solid mass transfer in a fixed-bed irrigated gas–liquid reactor with downward cocurrent flow. *Int. Chem. Eng.* **1982**, *22*, 244.

(70) Boelhouwer, J. G. Nonsteady operation of trickle bed reactors: hydrodynamics, mass and heat transfer. Ph.D. Thesis, Technische Universiteit Eindhoven, Eindhoven, The Netherlands, 2001.

(71) Chou, T. S.; Worley, F. L.; Luss, D. Local particle-liquid-phase mass transfer fluctuations in mixed-phase cocurrent downflow through a fixed bed in the pulsing regime. *Ind. Eng. Chem. Fundam.* **1979**, *18*, 279.

(72) Gabitto, J. F.; Lemcoff, N. O. Local solid–liquid mass transfer coefficients in a trickle-bed reactor. *Chem. Eng. J.* **1987**, *35*, 69.

(73) Gonzalez-Mendizabal, D.; Aguilera, M. E.; Pironti, F. Solid–liquid mass transfer and wetting factors in trickle bed reactors: Effect of the type of solid phase and the presence of chemical reaction. *Chem. Eng. Commun.* **1998**, *169*, 37.

(74) Herskowitz, M.; Abuelhaiza, M. Liquid–solid mass transfer in a trickle-bed reactor measured by means of a catalytic reaction. *Chem. Eng. Sci.* **1985**, *40*, 631.

(75) Highfill, S. W. Liquid–solid mass transfer coefficient in high-pressure trickle-bed reactor. Master's Thesis, Washington University, St. Louis, MO, 1998.

(76) Highfill, W.; Al-Dahhan, M. Liquid–solid mass transfer coefficient in high-pressure trickle bed reactors. *Trans. Inst. Chem. Eng.* **2001**, *79*, 631.

(77) Hirose, T.; Mori, Y.; Sato, Y. Liquid-to-particle mass transfer in fixed bed reactor with cocurrent gas–liquid downflow. *J. Chem. Eng. Jpn.* **1976**, *9*, 220.

(78) Lakota, A.; Levec, J. Solid–liquid mass transfer in packed beds with cocurrent downward two-phase flow. *AIChE J.* **1990**, *36*, 1444.

(79) Latifi, A. Analyse globale et locale des phénomènes de transfert de matière liquide-solide dans un réacteur à lit fixe fonctionnant à co-courant vers le bas de gaz et de liquide. Ph.D. Thesis, Institut National Polytechnique de Lorraine, Nancy, France, 1988.

(80) Latifi, M. A.; Laurent, A.; Storck, A. Liquid–solid mass transfer in a packed bed with downward cocurrent gas–liquid flow: an organic liquid phase with high Schmidt number. *Chem. Eng. J.* **1988**, *38*, 47.

(81) Lemay, Y.; Pineault, G.; Ruether, A. Particle-liquid mass transfer in a three-phase fixed bed reactor with cocurrent flow in the pulsing regime. *Ind. Eng. Chem. Process Des. Dev.* **1975**, *14*, 280.

(82) Leung, P. C.; Recasens, F.; Smith, J. M. Hydration of isobutene in a trickle bed reactor: wetting efficiency and mass transfer. *AIChE J.* **1987**, *33*, 996.

(83) Rao, V. G.; Drinkenburg, A. A. H. Solid–liquid mass transfer in packed beds with cocurrent gas–liquid downflow. *AIChE J.* **1985**, *31*, 1059.

(84) Ruether, J. A.; Ching-Shi, Y.; Hayduk, W. Particle mass transfer during cocurrent downward gas–liquid flow in packed beds. *Ind. Eng. Chem. Process Des. Dev.* **1980**, *19*, 103.

(85) Satterfield, C. N.; van Eek, N. W.; Bliss, G. S. Liquid–solid mass transfer in packed beds with downward concurrent gas–liquid flow. *AIChE J.* **1978**, *24*, 709.

(86) Sims, B. W.; Schulz, F. G.; Luss, D. Solid–liquid mass transfer to hollow pellets in a trickle bed. *Ind. Eng. Chem. Res.* **1993**, *32*, 1895.

(87) Specchia, V.; Baldi, G.; Gianetto, A. Solid−liquid mass transfer in concurrent two-phase flow through packed beds. *Ind. Eng. Chem. Process Des. Dev.* **1978**, *17*, 362.

(88) Tan, C. S.; Smith, J. M. A dynamic method for liquid-particle mass transfer in trickle beds. *AIChE J.* **1982**, *28*, 190.

(89) Yoshikawa, M.; Iwai, K.; Goto, S.; Teshima, H. Liquid−solid mass transfer in gas−liquid cocurrent flow through beds of small packings. *J. Chem. Eng. Jpn.* **1981**, *14*, 444.

(90) Gabitto, J. F.; Lemcoff, N. O. Wall mass transfer coefficient in a trickle bed reactor. *Chem. Eng. J.* **1985**, *30*, 23.

(91) Naderifar, A. Étude expérimentale locale et globale du transfer matière liquide/solide à la paroi d'un réacteur à lit fixe. Ph.D. Thesis, Institut National Polytechnique de Lorraine, Nancy, France, 1995.

(92) Latifi, M. A.; Naderifar, A.; Midoux, N. Experimental investigation of the liquid−solid mass transfer at the wall of a trickle-bed reactor—Influence of Schmidt number. *Chem. Eng. Sci.* **1997**, *52*, 4005.

(93) Latifi, M. A.; Naderifar, A.; Midoux, N. Energetic Analysis of the liquid-to-wall mass transfer in a trickle bed reactor. *Trans. Inst. Chem. Eng.* **1999**, *77*, 69.

(94) Rode, S. Analyse spatio-temporelle des phénomènes hydrodynamiques et de transfert de matière au sein d'un réacteur à lit fixe opérant en écoulement monophasique de liquide ou en co-courant vers le bas de gas et de liquide; Mise en œuvre de la technique des microsondes électrochimiques. Ph.D. Thesis, Institut National Polytechnique de Lorraine, Nancy, France, 1992.

(95) Rode, S.; Midoux, N.; Latifi, M. A. A. Storck, Hydrodynamics and liquid−solid mass transfer mechanisms in packed beds operating in cocurrent gas−liquid downflow: an experimental study using electrochemical shear rate sensors. *Chem. Eng. Sci.* **1994**, *49*, 1383.

(96) Rode, S.; Midoux, N.; Latifi, M. A.; Storck, A. Multiple hydrodynamic states in trickle beds operating in high-interaction regimes: liquid saturation and flow regime transitions. *Chem. Eng. Sci.* **1994**, *49*, 2535.

(97) Lara-Marquez, A. Les réacteurs à lit fixe à co-courrant vers le haut de gaz et de liquide. Étude du transfert de matière gaz−liquide. Ph.D. Thesis, Institut National Polytechnique de Lorraine, Nancy, France, 1992.

(98) Saada, M. Y. Assessment of interfacial area in co-current two-phase flow in packed beds. *Chim. Ind., Génie Chim.* **1972**, *105*, 1415.

(99) Fukushima, S.; Kusaka, K. Gas−Liquid mass transfer and hydrodynamic flow region in packed columns with cocurrent upward flow. *J. Chem. Eng. Jpn.* **1979**, *12*, 296.

(100) Specchia, V.; Sicardi, S.; Gianetto, A. Absorption in packed towers with concurrent upward flow. *AIChE J.* **1974**, *20*, 646.

(101) Ohshima, S.; Takematsu, T.; Kuriki, Y.; Shimada, K.; Suzuki, M.; Kato, J. Liquid-phase mass transfer coefficient and gas holdup in a packed-bed cocurrent up-flow column. *J. Chem. Eng. Jpn.* **1976**, *9*, 29.

(102) Molga, E. J.; Westerterp, K. R. Gas−liquid interfacial area and holdup in a cocurrent upflow packed bed bubble column reactor at elevated pressures. *Ind. Eng. Chem. Res.* **1997**, *36*, 622.

(103) Voyer, R. D.; Miller, A. I. Improved gas−liquid contacting co-current flow. *Can. J. Chem. Eng.* **1968**, *46*, 335.

(104) Lara-Marquez, A.; Wild, G.; Laurent, A.; Midoux, N. Coefficient de transfert de matière gaz-liquide dans un réacteur catalytique à lit fixe fonctionnant à co-courant vers le haut de gaz et de liquide en présence de systèmes coalescents ou inhibiteurs de coalescence et/ou visqueux. In *Récents Progrès Génie Procédés*; Jallut, C., Ed.; Lavoisier, Techniques et Documentation: Paris, 1993; Vol. 30, pp 67−72.

(105) Lara-Marquez, A.; Wild, G.; Midoux, N. A review of recent chemical techniques for the determination of the volumetric mass-transfer coefficient k_La in gas−liquid reactors. *Chem. Eng. Process.* **1994**, *33*, 247.

(106) Goto, S.; Saikawa, K.; Gaspillo, P. D. Mass transfer and holdup in gas−liquid cocurrent flow packed beds containing water repellent particles. *Can. J. Chem. Eng.* **1991**, *69*, 1344.

(107) Syaiful, S. Réacteurs polyphasiques à cocourant ascendant: Influence de la viscosité sur les rétentions, dispersions axiales et tranfert gaz−liquide. Ph.D. Thesis, Institut National Polytechnique de Toulouse, Toulouse, France, 1992.

(108) Syaiful, S.; Wilhelm, A. M.; Svensen, H. F.; Delmas, H. Upward cocourrent gas−liquid−(solid) contactors: Holdup, axial dispersions, gas−liquid mass transfer. *Trans. Inst. Chem. Eng.* **1995**, *73*, 643.

(109) Stüber, F. Sélectivité en réacteur catalytique triphasique: Analyse expérimentale et théorique d'hydrogénations consécutives en lit fixe catalytique à co-courant ascendant de gaz et de liquide. Ph.D. Thesis, Institut National Polytechnique de Toulouse, Toulouse, France, 1995.

(110) Stüber, F.; Wilhelm, A. M.; Delmas, H. Modeling of three-phase catalytic upflow reactor: A significant chemical determination of liquid−solid and gas−liquid mass transfer coefficients. *Chem. Eng. Sci.* **1996**, *51*, 2161.

(111) Storck, A.; Latifi, M. A.; Barthole-Delaunay, G.; Laurent, A.; Charpentier, J.-C. Electrochemical study of liquid−solid mass transfer in packed bed electrodes with upward and downward cocurrent gas−liquid flow. *J. Appl. Electrochem.* **1986**, *16*, 947.

(112) Delauney, G.; Storck, A.; Laurent, A.; Charpentier, J. C. Electrochemical study of liquid−solid mass transfer in packed beds with upward cocurrent gas−liquid flow. *Ind. Eng. Chem. Process Des. Dev.* **1980**, *19*, 514.

(113) Colquhoun-Lee, I.; Stepanek, J. B. Solid−liquid mass transfer in two phase co-current upward flow in packed beds. *Trans. Inst. Chem. Eng.* **1978**, *56*, 136.

(114) Kirillov, V. A.; Nasamanyan, M. A. Mass transfer processes between liquid and packing in a three-phase fixed bed. *Int. Chem. Eng.* **1976**, *16*, 538.

(115) Mochizuki, S.; Matsui, T. Liquid−solid mass transfer in liquid−gas upward cocurrent flow packed beds. *Chem. Eng. Sci.* **1974**, *29*, 1328.

(116) Nikov, I.; Delmas, H. Solid−liquid mass transfer in three-phase fixed and fluidized beds. *Chem. Eng. Sci.* **1987**, *42*, 1089.

(117) Yasunishi, A.; Fukuma, M.; Muroyama, K. Wall-to-liquid mass transfer in packed and fluidized beds with gas−liquid concurrent upflow. *J. Chem. Eng. Jpn.* **1988**, *21*, 522.

(118) Crine, M. Heat transfer phenomena in trickle-bed reactors. *Chem. Eng. Commun.* **1982**, *19*, 99.

(119) Colli-Serrano, M. T. Hydrodynamique et transfert de chaleur dans un réacteur à lit fixe gaz−liquide−solide. Ph.D. Thesis, Institut National Polytechnique de Lorraine, Nancy, France, 1993.

(120) Specchia, V.; Baldi, G. Heat transfer in trickle-bed reactors. *Chem. Eng. Commun.* **1979**, *3*, 483.

(121) Matsuura, A.; Hitaka, Y.; Akehata, T.; Shirai, T. Effective radial thermal conductivity in packed beds with downward cocurrent gas−liquid flow. *Heat Transfer—Jpn. Res.* **1979**, *8*, 44.

(122) Hashimoto, K.; Muroyama, K.; Fujiyoshi, K.; Nagata, S. Effective radial thermal conductivity in cocurrent flow of a gas and liquid through a packed bed. *Int. Chem. Eng.* **1976**, *16*, 720.

(123) Hashimoto, K.; Muroyama, K.; Fujiyoshi, K.; Nagata, S. Radial effective thermal conductivity in gas−liquid cocurrent flow through packed beds. *Heat Transfer—Jpn. Res.* **1977**, *6*, 44.

(124) Lamine, A. S.; Gerth, L.; Le Gall, H.; Wild, G. Heat transfer in a packed bed reactor with cocurrent downflow of a gas and a liquid. *Chem. Eng. Sci.* **1996**, *51*, 3813.

(125) Nakamura, M.; Tanahashi, T.; Takada, D.; Ohsasa, K.; Sugiyama, S. Heat transfer in a packed bed with gas−liquid cocurrent upflow. *Heat Transfer—Jpn. Res.* **1981**, *10*, 92.

(126) Weekman, V. W. Heat transfer and fluid flow for concurrent, gas−liquid flow in packed beds. Ph.D. Thesis, Purdue University, West Lafayette, IN, 1963.

(127) Weekman, V. W.; Myers, J. E. Heat transfer characteristics of concurrent gas−liquid flow in packed beds. *AIChE J.* **1965**, *11*, 13.

(128) Matsuura, A.; Hitaka, Y.; Akehata, T.; Shirai, T. Apparent wall heat transfer coefficient in packed beds with downward cocurrent gas−liquid flow. *Heat Transfer—Jpn. Res.* **1979**, *8*, 53.

(129) Muroyama, K.; Hashimoto, K.; Tomita, T. Heat transfer from the wall in gas−liquid cocurrent packed beds. *Heat Transfer—Jpn. Res.* **1978**, *7*, 87.

(130) Marcandelli, C. Hydrodynamique, transfert de chaleur particule-fluide et distribution des phases dans les réacteurs à lit fixe à écoulement descendant de gaz et de liquide. Ph.D. Thesis, Institut National Polytechnique de Lorraine, Nancy, France, 1999.

(131) Marcandelli, C.; Wild, G.; Lamine, A. S.; Bernard, J. R. Measurement of local particle-fluid heat transfer coefficient in trickle-bed reactors. *Chem. Eng. Sci.* **1999**, *54*, 4997.

(132) Boelhouwer, J. G.; Piepers, H. W.; Drinkenburg, A. A. Particle-liquid heat transfer in trickle bed reactors. *Chem. Eng. Sci.* **2001**, *56*, 1181.

(133) Gutsche, S. Transfert de chaleur dans un réacteur à lit fixe à co-courant ascendant de gaz et de liquide. Ph.D. Thesis, Institut National Polytechnique de Lorraine, Nancy, France, 1990.

(134) Lamine, A. S.; Colli-Serrano, M. T.; Wild, G. Hydrodynamics and heat transfer in packed beds with liquid upflow. *Chem. Eng. Process.* **1992**, *31*, 385.

(135) Lamine, A. S.; Colli-Serano, M. T.; Wild, G. Influence of viscosity and foaming properties on heat transfer in packed bed with cocurrent upflow of gas and liquid. *Trans. Inst. Chem. Eng.* **1995**, *73*, 280.

(136) Lamine, A. S.; Colli-Serano, M. T.; Wild, G. Heat transfer in a packed bed with gas–liquid cocurrent upflow. *Chem. Eng. Sci.* **1992**, *47*, 3493.

(137) Colli-Serano, M. T.; Midoux, N. Hydrodynamics and heat transfer in packed beds with cocurrent upflow for coalescing and noncoalescing liquids. A simple model. *Chem. Eng. Sci.* **2000**, *55*, 4149.

(138) Iliuta, I.; Larachi, F.; Grandjean, B. P. A.; Wild, G. Gas–liquid interfacial mass transfer in trickle-bed reactors: State-of-the-art correlations. *Chem. Eng. Sci.* **1999**, *54*, 5633.

(139) Bensetiti, Z.; Larachi, F.; Grandjean, B. P. A.; Wild, G. Liquid saturation in cocurrent upflow fixed-bed reactors: A state-of-the-art correlation. *Chem. Eng. Sci.* **1997**, 52, 4239.

(140) Larachi, F.; Bensetiti, Z.; Grandjean, B. P. A.; Wild, G. Two-phase frictional pressure drop in flooded-bed reactors: A state-of-the-art correlation. *Chem. Eng. Technol.* **1998**, *21*, 887.

(141) Cloutier, P.; Tibirna, C.; Grandjean, B. P. A.; Thibault, J. Nnfit, logiciel de régression utilisant les réseaux à couches. http://www.gch.ulaval.ca/∼nnfit, 1996.

(142) Press, W. H.; Teukolsky, S. A.; Vetterling, W. T.; Flannery, B. P. *Numerical recipes in Fortran. The art of scientific computing*, 2nd ed.; Cambridge University Press: Cambridge, MA, 1992.

(143) Wild, G.; Larachi, F.; Charpentier, J. C. Heat and mass transfer in gas–liquid–solid fixed bed reactors. In *Heat and mass transfer in porous media*; Quintard, M., Todorovic, M., Eds.; Elsevier: Amsterdam, The Netherlands, 1987; p 616.

(144) Reiss, L. P. Cocurrent gas–liquid contacting in packed columns. *Ind. Eng. Chem. Process Des. Dev.* **1967**, *6*, 486.

(145) Takahashi, K. M.; Alkire, R. C. Mass transfer from dispersed bubbles to electrolyte solutions in packed beds. *AIChE J.* **1988**, *34*, 1504.

(146) Turpin, J. L.; Huntington, R. L. Prediction of pressure drop for two phase, two-components concurrent flow in packed beds. *AIChE J.* **1967**, *13*, 1196.

(147) Dharwadkar, A.; Sylvester, N. D. Liquid–solid mass transfer in trickle beds, *AIChE J.* **1977**, *23*, 376.

(148) Burghardt, A.; Bartelmus, G. Hydrodynamics and mass transfer in three-phase cocurrent reactors. *Chem. Eng. Sci.* **1996**, *51*, 2733.

(149) Kikuchi, K.-I.; Sugawara, T.; Ohashi, H. Correlation of liquid-side mass transfer coefficient based on the new concept of specific power group. *Chem. Eng. Sci.* **1988**, *43*, 2533.

(150) Jadhav, S. V.; Pangarkar, V. G. Solid–Liquid mass transfer in packed bubble columns. *Chem. Eng. Sci.* **1990**, *45*, 1139.

(151) Sokolov, V. N.; Yablokova, M. Thermal conductivity of a stationary granular bed with upward gas–liquid flow. *J. Appl. Chem. USSR* **1983**, *56*, 551.

(152) Chu, C. F.; Ng, K. M. Effective thermal conductivity in trickle-bed reactors: Application of effective medium and random walk analysis. *Chem. Eng. Commun.* **1985**, *37*, 127.

(153) Bartelmus, G. Local solid–liquid mass transfer coefficients in a three-phase fixed bed reactor. *Chem. Eng. Process.* **1989**, *26*, 111.

(154) Grosser, K.; Carbonell, R. G.; Cavero, A.; Saez, A. E. Lateral thermal dispersion in gas–liquid cocurrent downflow through packed beds. *AIChE J.* **1996**, *42*, 2977.

(155) Coppola, L.; Cavatorta, O. N.; Bohm, U. Mass transfer to volumetric electrodes with two phase flow. *J. Appl. Electrochem.* **1989**, *19*, 100.

(156) Mochizuki, S. Mass transport phenomena and hydrodynamics in packed beds with gas–liquid concurrent upflow. *AIChE J.* **1978**, *24*, 1138.

(157) *L'Air Liquide, Encyclopédie des gaz*; Elsevier: Amsterdam, The Netherlands, 1976.

(158) Reid, R. C.; Prausnitz, J. M.; Poling, B. E. *The Properties of Gases and Liquids*, 4th ed.; McGraw-Hill: New York, 1987.

(159) *International Critical Tables of Numerical Data, Physics, Chemistry and Technology*; McGraw-Hill Book Co.: New York, 1929; Vol. V.

(160) Lide, D. R. *Handbook of Chemistry and Physics*, 73rd ed.; 1993.

(161) Mariani, N. J.; Martinez, O. M.; Barreto, G. F. Evaluation of heat transfer parameters in packed beds with cocurrent downflow of liquid and gas. *Chem. Eng. Sci.* **2001**, *56*, 5995.

Received for review June 4, 2002
Revised manuscript received October 4, 2002
Accepted October 15, 2002

IE020416G